Article

Molecular Cell

# The Co-chaperone Cns1 and the Recruiter Protein Hgh1 Link Hsp90 to Translation Elongation via Chaperoning Elongation Factor 2

## Graphical Abstract

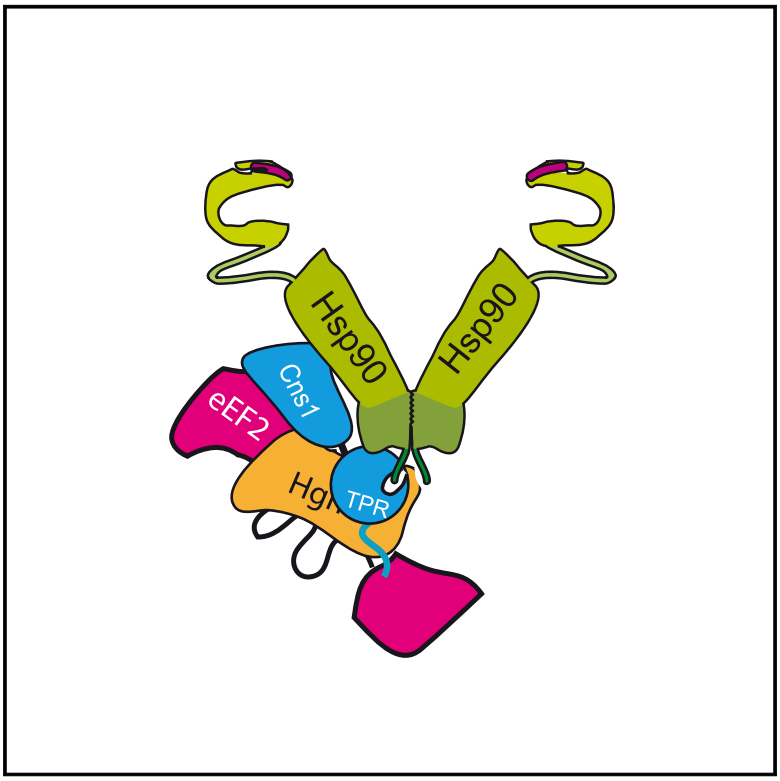


## Authors

Florian H. Schopf, Eva M. Huber, Christopher Dodt, ..., Michael Sattler, Michael Groll, Johannes Buchner

## Correspondence

johannes.buchner@tum.de

## In Brief

The Hsp90 co-chaperone Cns1 consists of three domains: an unfolded region, a TPR domain, and a domain with a novel fold. The disordered region is essential *in vivo*. Together with the newly identified recruiter protein Hgh1, it regulates the folding and stability of the elongation factor eEF2 in yeast.

## Highlights

- Cns1 contains a disordered region, a TPR domain, and a domain with a novel fold
- Cns1's essential function is associated with protein translation
- Cns1, Hgh1, and Hsp90 form a complex with eEF2
- The Cns1 complex including the co-factor Hgh1 chaperones eEF2

Schopf et al., 2019, Molecular Cell *74*, 1–15
April 4, 2019 
https://doi.org/10.1016/j.molcel.2019.02.011

CellPress

Please cite this article in press as: Schopf et al., The Co-chaperone Cns1 and the Recruiter Protein Hgh1 Link Hsp90 to Translation Elongation via Chaperoning Elongation Factor 2, Molecular Cell (2019), https://doi.org/10.1016/j.molcel.2019.02.011

Molecular Cell
Article

# The Co-chaperone Cns1 and the Recruiter Protein Hgh1 Link Hsp90 to Translation Elongation via Chaperoning Elongation Factor 2

Florian H. Schopf,[1] Eva M. Huber,[1] Christopher Dodt,[1] Abraham Lopez,[1,2] Maximilian M. Biebl,[1] Daniel A. Rutz,[1] Moritz Mühlhofer,[1] Gesa Richter,[1,3] Tobias Madl,[1,3,4] Michael Sattler,[1,2] Michael Groll,[1] and Johannes Buchner[1,5,*]
[1]Center for Integrated Protein Science at the Department Chemie, Technische Universität München, Lichtenbergstrasse 4, 85748 Garching, Germany
[2]Institute of Structural Biology, Helmholtz Zentrum München, 85764 Neuherberg, Germany
[3]Gottfried Schatz Research Center, Medical University of Graz, 8036 Graz, Austria
[4]BioTechMed-Graz, 8010 Graz, Austria
[5]Lead Contact
*Correspondence: johannes.buchner@tum.de
https://doi.org/10.1016/j.molcel.2019.02.011

## SUMMARY

**The Hsp90 chaperone machinery in eukaryotes comprises a number of distinct accessory factors. Cns1 is one of the few essential co-chaperones in yeast, but its structure and function remained unknown. Here, we report the X-ray structure of the Cns1 fold and NMR studies on the partly disordered, essential segment of the protein. We demonstrate that Cns1 is important for maintaining translation elongation, specifically chaperoning the elongation factor eEF2. In this context, Cns1 interacts with the novel co-factor Hgh1 and forms a quaternary complex together with eEF2 and Hsp90. The *in vivo* folding and solubility of eEF2 depend on the presence of these proteins. Chaperoning of eEF2 by Cns1 is essential for yeast viability and requires a defined subset of the Hsp90 machinery as well as the identified eEF2 recruiting factor Hgh1.**

## INTRODUCTION

In the eukaryotic cytosol, the Hsp90 chaperone machinery is a conserved regulator of protein conformation (Schopf et al., 2017). The growing list of Hsp90 clients contains many protein kinases, transcription factors, and steroid hormone receptors, among others (https://www.picard.ch/downloads/Hsp90interactors.pdf). ATP binding and hydrolysis drive large conformational rearrangements in the Hsp90 dimer. During the chaperone cycle, Hsp90 transits from a V-shaped open conformation to a closed state via several intermediates (Ali et al., 2006; Hessling et al., 2009; Shiau et al., 2006).

Hsp90 function is regulated by a large cohort of conserved co-chaperones (Johnson, 2012; Mayer and Le Breton, 2015). They can either act as modulators of the Hsp90 chaperone cycle or facilitate client recruitment and processing. For example, Aha1 increases the Hsp90 ATPase activity (Panaretou et al., 2002; Retzlaff et al., 2010), whereas Sti1 inhibits the ATPase (Li et al., 2011; Panaretou et al., 1998; Richter et al., 2003); additionally, it connects Hsp90 with Hsp70 (Johnson et al., 1998; Scheufler et al., 2000; Schmid et al., 2012). Of the 12 known co-chaperones in yeast, only 3, namely Cdc37, Sgt1, and Cns1, are essential (Johnson, 2012). Cdc37 is involved in kinase maturation (Brugge, 1986), and Sgt1 supports kinetochore assembly (Catlett and Kaplan, 2006; Kitagawa et al., 1999). The essential role of Cns1 is still enigmatic. Cns1 was discovered as a multi-copy suppressor for Hsp90 loss-of-function mutations (Nathan et al., 1999). Moreover, the Hsp90 co-chaperones Cns1 and Cpr7 have overlapping but undefined *in vivo* functions (Dolinski et al., 1998; Marsh et al., 1998; Tesic et al., 2003; Zuehlke and Johnson, 2012). *In vitro* studies showed that Cns1 binds to both Hsp90 and Hsp70 (Hainzl et al., 2004). Furthermore, Cns1 and Cpr7 interact weakly with the 80S ribosome, and *cns1* and *cpr7Δ* mutants are sensitive to the translation inhibitor hygromycin B (Albanèse et al., 2006; Tenge et al., 2015).

In this study, we solved the structure of Cns1 and identified the N-terminal, mostly unstructured region to be essential *in vivo*. Together, Cns1 and the co-factor Hgh1 are crucial for the folding and stability of the translation elongation factor eEF2 *in vivo* and thus connect the Hsp90 machinery to protein translation.

## RESULTS

### Cns1 Harbors a Unique Two-Domain Structure Linked by a Long Helix

The Hsp90 co-chaperone Cns1 is an essential protein in *S. cerevisiae* (Dolinski et al., 1998; Marsh et al., 1998) with a unique sequence (Figure S1A). To determine its three-dimensional structure, we initially focused on a Cns1 construct harboring residues 221–385, since previous work had shown that its C domain crystallizes (Stanitzek, 2005). Its structure was solved at 1.55 Å resolution applying anomalous phasing via seleno-methionine labeling ($R_{free}$ 18.6%; PDB ID: 6HFM; Figure 1A; Table 1); the two molecules per asymmetric unit have a root-mean-square deviation (RMSD) of 0.31 Å (Figure S1C). We also determined the crystal structure of the C

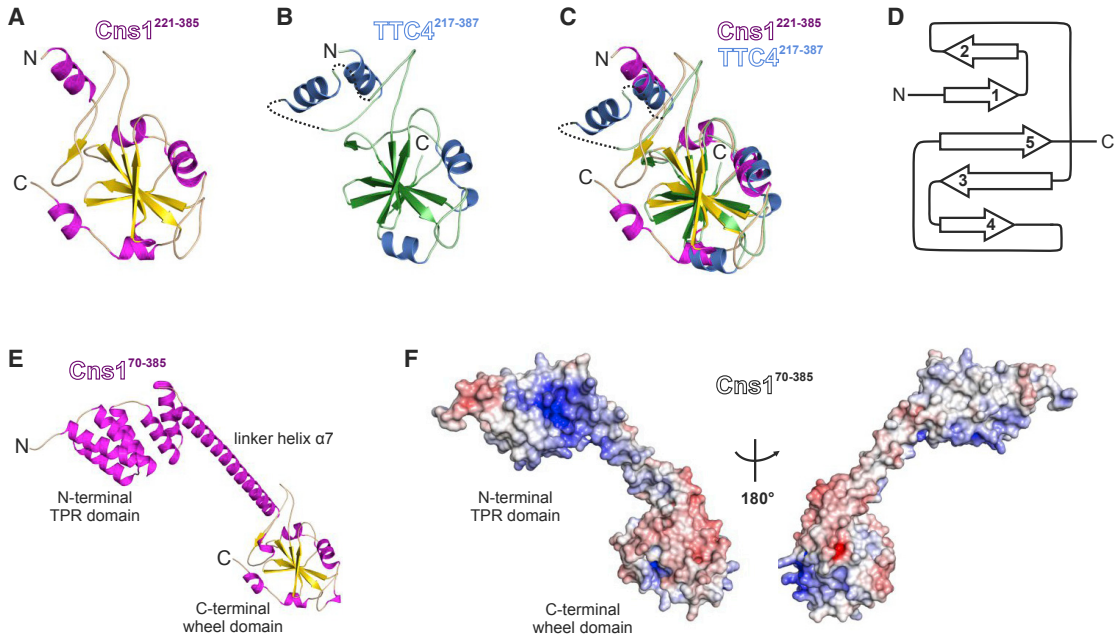


**Figure 1. Crystal Structures of Yeast Cns1 and Human TTC4**

(A) Ribbon plot of the C-terminal wheel domain of yeast Cns1 (residues 221–385). The central β sheet structure is colored in yellow, while the surrounding helices are depicted in magenta.

(B) Ribbon plot of the C-terminal domain of human TTC4 (residues 217–387). β sheets are highlighted in green and helices in blue. Loops disordered in the crystal lattice are shown as black dotted lines.

(C) Superposition of Cns1$^{221–385}$ shown in (A) and TTC4$^{217–387}$ depicted in (B).

(D) Topology plot of the conserved, twisted β sheet of the C-terminal domains of Cns1 and TTC4. Helices have been omitted from this plot for clarity. For an overall and a more detailed topology plot, see Figure S1B.

(E) The Cns1$^{70–385}$ crystal structure shown as ribbon visualizes the two-domain architecture of the protein. Color coding is according to (A).

(F) Surface charge distributions for Cns1$^{70–385}$ at pH 7. The left illustration corresponds to the orientation shown in (E), while the right is rotated by 180°. Surface colors indicate positive and negative electrostatic potentials colored from 10 kT/e (intense blue) to −10 kT/e (intense red). The blue-colored pocket of the TPR domain corresponds to the binding site for the Hsp90 C terminus (Figure S1G).

domain of the human Cns1 homolog TTC4 (tetratricopeptide repeat protein 4; residues 217–387) at 1.65 Å resolution by molecular replacement using the yeast coordinates ($R_{free}$ 18.95%; PDB: 6HFO; Figure 1B; Table 1). Despite low sequence conservation (18% sequence identity and 37% sequence similarity) between yeast Cns1$^{221–385}$ and human TTC4$^{217–387}$ (Figure S1A), both domains adopt the same overall fold consisting of a twisted five-stranded β sheet surrounded by several α helices (RMSD 1.40 Å; Figure 1C). While the α helices are variable, the central β sheet is well conserved. It is formed by two two-stranded antiparallel β sheets with the fifth strand acting as the bridging element (Figure 1D). A Dali search (Holm and Rosenström, 2010) revealed that this tertiary structure is not related to any other protein topology known to date. According to the shape of its 2D projection, we propose the name "wheel domain" for it (Figure 1C).

N-terminal truncations, protein stability improvements, and extensive screening of crystallization conditions allowed us to determine the structure of Cns1$^{70–385}$ to 2.8 Å resolution. Patterson calculations using the coordinates of the C domain (Cns1$^{221–385}$) as a search model indicated additional electron density. By iterative model building and refinement, we could place all amino acids except for the first four residues in the $2F_O$-$F_C$ electron density map ($R_{free}$ 28.8%; PDB: 6HFT; Table 1). Cns1$^{70–385}$ folds into an N-terminal tetratricopeptide repeat (TPR) domain of three units, i.e., six antiparallel α helices (α1–α6) and the C domain connected by a straight helix (termed α7) of 44 amino acids (Figures 1E and S1B). Both domains are arranged in *trans* relatively to the α7 helix (Figure S1D). Notably, the structure of the C domain is unaltered compared to Cns1$^{221–385}$ (RMSD 0.43 Å; Figure S1E). The TPR domain known to interact with the C-terminal EEVD sequence of Hsp90 (Russell et al., 1999; Scheufler et al., 2000) is structurally closely related to that of the FK506-binding protein 51 (FKBP51) (Sinars et al., 2003) (Dali search: *Z* score 17, RMSD 1.9 Å, identity 27%) and the RNA Polymerase II-associated protein 3 (RPAP3) (Pal et al., 2014) (*Z* score 16.7, RMSD 2.7, identity 28%), as well as other TPR motifs (Figure S1F).

Although Cns1$^{70–385}$ was crystallized in the presence of 1.5-fold molar excess of MEEVD, the peptide is not defined in the electron density map. We therefore mapped the binding site by superimposing Cns1$^{70–385}$ onto the RPAP3 crystal structure in complex with the peptide SRMEEVD (PDB: 4CGW) (Pal et al., 2014). According to this model, the MEEVD sequence fits into a cradle-shaped groove of the Cns1 TPR domain (Figures 1F and S1G). The conserved residues Lys87, Lys156, and

Please cite this article in press as: Schopf et al., The Co-chaperone Cns1 and the Recruiter Protein Hgh1 Link Hsp90 to Translation Elongation via Chaperoning Elongation Factor 2, Molecular Cell (2019), https://doi.org/10.1016/j.molcel.2019.02.011



**Table 1. X-Ray Data Collection and Refinement Statistics**

| | $Cns1^{221–385}$ | $Cns1^{221–385\_Se}$ | $TTC4^{217–387}$ | $Cns1^{70–385}$ |
|---|---|---|---|---|
| Crystal Parameters | | | | |
| Space group | $P2_12_12_1$ | $P2_12_12_1$ | C2 | $P4_12_12$ |
| Cell constants | a = 45.0 Å<br>b = 79.0 Å<br>c = 98.9 Å | a = 44.9 Å<br>b = 81.6 Å<br>c = 100.6 Å | a = 94.7 Å<br>b = 42.8 Å<br>c = 43.1 Å<br>β = 93.6° | a = 50.8 Å<br>b = 50.8 Å<br>c = 283.1 Å |
| Molecules/AU[a] | 2 | 2 | 1 | 1 |
| Data Collection | | | | |
| Beam line | X06SA, SLS | X06DA, SLS | ID30B, ESRF | X06SA, SLS |
| Wavelength (Å) | 1.0 | 0.97939 | 0.97856 | 0.97793 |
| Resolution range (Å)[b] | 40–1.55 (1.65–1.55) | 40–2.1 (2.2–2.1) | 45–1.65 Å (1.75–1.65 Å) | 40–2.8 (2.9–2.8) |
| No. observations | 302,101 | 283,690 | 60,396 | 45,729 |
| No. unique reflections[c] | 51,808[d] | 41,661[e] | 20,421[d] | 9,753[d] |
| Completeness (%)[b] | 99.7 (99.7) | 100.0 (100.0) | 97.7 (97.9) | 97.9 (99.8) |
| $R_{merge}$ (%)[b,f] | 4.5 (53.6) | 8.2 (51.0) | 4.4 (57.7) | 8.3 (61.3) |
| I/σ (I)[b] | 18.1 (3.4) | 15.7 (3.5) | 12.8 (1.9) | 10.6 (2.2) |
| Refinement (REFMAC5) | | | | |
| Resolution range (Å) | 15–1.55 | | 15–1.65 | 15–2.8 |
| No. reflections working set | 49,149 | | 19,370 | 9,187 |
| No. reflections test set | 2,587 | | 1,019 | 484 |
| No. non-hydrogen | 3,003 | | 1,354 | 2,554 |
| Solvent ($H_2O$, $Mg^{2+}$, $PO_4^{3-}$) | 307 | | 81 | 12 |
| $R_{work}/R_{free}$ (%)[g] | 16.0/18.6 | | 15.9/18.9 | 25.9/28.8 |
| RMSD bond (Å)/(°)[h] | 0.007/1.2 | | 0.006/1.2 | 0.007/1.0 |
| Average B factor ($Å^2$) | 27.5 | | 42.7 | 87.5 |
| Ramachandran plot (%)[i] | 99.7/0.3/0.0 | | 99.3/0.7/0.0 | 98.4/1.6/0.0 |
| | PDB: 6HFM | | PDB: 6HFO | PDB: 6HFT |

[a]Asymmetric unit
[b]The values in parentheses for resolution range, completeness, $R_{merge}$, and I/σ (I) correspond to the highest-resolution shell
[c]Data reduction was carried out with XDS and from a single crystal
[d]Friedel pairs were treated as identical reflections
[e]Friedel pairs were treated as individual reflections
[f]$R_{merge}(I) = \Sigma_{hkl}\Sigma_j \mid I(hkl)_j - < I(hkl)> \mid / \Sigma_{hkl}\Sigma_j I(hkl)_j$, where $I(hkl)_j$ is the $j^{th}$ measurement of the intensity of reflection hkl and <I(hkl)> is the average intensity
[g]$R = \Sigma_{hkl} \mid \mid F_{obs}\mid - \mid F_{calc}\mid \mid / \Sigma_{hkl} \mid F_{obs}\mid$, where $R_{free}$ is calculated without a sigma cut off for a randomly chosen 5% of reflections, which were not used for structure refinement, and $R_{work}$ is calculated for the remaining reflections
[h]Deviations from ideal bond lengths/angles
[i]Percentage of residues in favored region/allowed region/outlier region

Arg160 (Figure S1A) may provide the peptide binding site. During crystallization, the arrangement of $Cns1^{70–385}$ in the lattice likely caused displacement of the MEEVD peptide due to steric hindrance (Figure S1H).

The exceptional domain arrangement of $Cns1^{70–385}$ raised the question whether the long linker helix α7 is fixed in its orientation. Arg234 at the C-terminal end of the linker helix hydrogen bonds to residues of the wheel domain, i.e., to the main-chain oxygen atoms of Phe261 and Ser263 as well as to the side chain of Glu287, and might fix the orientation of the α7 helix relative to the C domain (Figure S1I). However, since mutations of Arg234 and Glu287 (Figure S1A) did not provoke a phenotype in yeast, we conclude that either the domains are held in place despite the mutations or a fixed domain arrangement is not essential for the function of Cns1.

## The N-Terminal Segment of Cns1 Is Essential for Yeast Viability

To determine the parts of the protein essential for its function in yeast, we expressed Cns1 variants in a *cns1*Δ knockout strain (Figures 2 and S2A). In agreement with the literature (Tesic et al., 2003), yeast cells expressing C-terminal truncations of Cns1 ($Cns1^{1–220}$, $Cns1^{1–200}$, $Cns1^{1–190}$, and $Cns1^{1–185}$) were viable, and cells expressing the C domain ($Cns1^{169–385}$, $Cns1^{191–385}$, and $Cns1^{221–385}$) were inviable (Figures 2 and S2B–S2D). Truncation of the N domain of Cns1 ($Cns1^{36–385}$) showed no obvious growth defect. However, deletion of the first 40 amino acids ($Cns1^{41–385}$) resulted in severe sickness, and removal of more than 44 amino acids ($Cns1^{46–385}$ and $Cns1^{51–385}$) was lethal. When we depleted the C domain from a construct lacking the N-terminal 35 residues that support

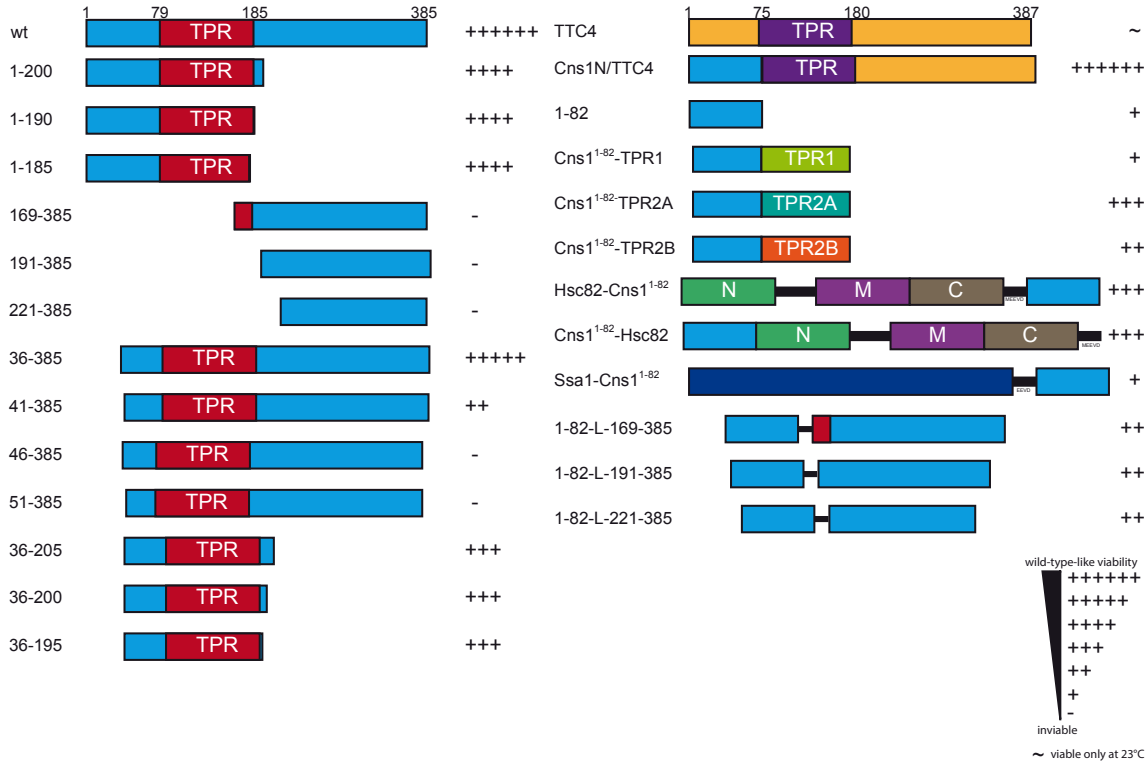


**Figure 2. Cns1 Is an Essential Hsp90 Co-chaperone in Yeast**

Schematic representation of Cns1 key mutants, Hsp90, TTC4, and chimeras used in 5′-FOA shuffling experiments. "+"-graduation indicates cell viability, starting with "++++++" for WT-like growth and ceasing with "−" for lethality. "∼" indicates cell viability at 23°C.

wild-type (WT)-like viability ($Cns1^{36–205}$, $Cns1^{36–200}$, and $Cns1^{36–195}$), the cells were also very sick, indicating that in the absence of the first 35 residues, the C domain is crucial *in vivo* (Figures 2 and S2B–S2D).

It had been reported that Cns1 can be replaced in yeast by its human ortholog TTC4 (Kachroo et al., 2015). In our assays, however, TTC4 did not complement at 30°C; at 23°C, cells exhibited severely reduced growth (Figures 2, S2D, and S2J). The sequences of Cns1 and TTC4 differ mainly in the N domain (Figure S1A). A chimera consisting of the Cns1 N domain and the TTC4 TPR+C domains was viable like $Cns1^{WT}$. Thus, Cns1 is structurally and functionally conserved from yeast to man. Interestingly, the Cns1 N domain alone, $Cns1^{1–82}$, still conferred viability but exhibited a severe growth defect (Figure S2F).

As Cns1 binds to both Hsp90 and Hsp70 via its TPR domain (Hainzl et al., 2004), we determined which interaction is crucial *in vivo*. To this end, we fused the N domain ($Cns1^{1–82}$) to the TPR1, TPR2A, or TPR2B domains of the co-chaperone Sti1, which are known to interact with Hsp90 (TPR2A and TPR2B) or Hsp70 (TPR1 and TPR2B) (Scheufler et al., 2000; Schmid et al., 2012). The fusion to TPR2A improved cell growth ($Cns1^{1–82\text{-}TPR2A}$), whereas $Cns1^{1–82\text{-}TPR1}$-expressing cells grew comparable to $Cns1^{1–82}$ alone and $Cns1^{1–82\text{-}TPR2B}$ gave an intermediate phenotype (Figures 2, S2A, S2E, and S2F). Thus Cns1's essential function is associated with Hsp90. To further test this assumption, we fused the N-terminal 82 amino acids of Cns1 in frame to both Hsp90 ($Cns1^{1–82}$-Hsc82 and Hsc82-$Cns1^{1–82}$) and Hsp70 (Ssa1-$Cns1^{1–82}$). Strikingly, only the fusion to Hsp90 improved cell growth compared to the $Cns1^{1–82}$ construct (Figures 2 and S2G).

To address the function of the C domain in more detail, we constructed mutants where the TPR domain is replaced by a flexible linker ($Cns1^{1–82\text{-}L\text{-}169–385}$, $Cns1^{1–82\text{-}L\text{-}191–385}$, and $Cns1^{1–82\text{-}L\text{-}221–385}$). The C domain improved the viability of the mutants, even in the absence of the TPR module (Figures 2, S2A, and S2I).

The overexpression of selected Cns1 mutants affects yeast growth as well. Interestingly, only overexpression of the $Cns1^{51–385}$ mutant in wild-type yeast led to a dominant-negative phenotype underlining the functional interplay between the three domains (Figure S2H).

## The Essential N-Terminal Segment of Cns1 Is Intrinsically Disordered and Contains Two Helical Regions That Interact with Its TPR Domain

SAXS experiments (Figure S3A–S3C) confirmed that Cns1 contains two stable domains, as two maxima were observed. The first maximum corresponds to the radius of gyration ($R_g$) of the isolated domains, and the second maximum is related to the distance between their centers of mass. However, comparison of the experimental data with the SAXS data back-calculated from the crystal structure indicates that the domains adopt a

flexible orientation in solution (Figure S3B). Comparison of the SAXS data for truncation mutants, i.e., Cns1$^{1–220}$ and Cns1$^{70–220}$, suggests that the Cns1 N domain is disordered, as the pairwise distribution function of Cns1$^{1–220}$ shows a tail (80–110 Å) in addition to the single maximum characteristic for disordered regions (Figure S3B). *Ab initio* modeling confirms the structure of Cns1 in solution as obtained by crystallography but indicates flexibility in the connecting helix (Figure S3C).

To characterize the N domain structurally, we performed NMR spectroscopy. Initially, we analyzed Cns1$^{1–82}$ and the isolated TPR domain (Cns1$^{70–205}$). The NMR chemical shifts in $^{1}$H, $^{15}$N HSQC spectra of Cns1$^{1–82}$ (Figure 3A) show low dispersion and narrow linewidths, demonstrating that the N domain is intrinsically disordered. However, analysis of secondary $^{13}$C chemical shifts (Wishart and Sykes, 1994) using TALOS+ (Shen et al., 2009) revealed two regions (residues 38–43 and 67–70) with helical propensity (Figure 3B). Residual structures in these regions are further supported by positive {$^{1}$H}-$^{15}$N heteronuclear NOE values (Farrow et al., 1994b), while the other parts of the construct have low or negative values, indicating high flexibility (Figure 3B).

Next, we determined whether the N domain could transiently interact with the TPR domain by titrating $^{15}$N-labeled Cns1$^{1–82}$ with unlabeled Cns1$^{70–205}$ and vice versa (Figures 3A and 3C). NMR signals of several residues in either protein show significant chemical shift perturbations (CSPs) and/or intense line broadening, indicating interaction. Notably, residues with large CSPs in the N-terminal segment correspond to the helical regions that harbor several negatively charged residues (Figure 3B).

## Cns1 Interacts with Hsp90 via Its TPR Domain

As many co-chaperones interact preferentially with specific conformations of Hsp90, we tested binding of Cns1 to Hsp90 by analytical ultracentrifugation (AUC) in the presence of ATP, ADP, or the non-hydrolyzable analog AMP-PNP, which leads to a closed conformation of Hsp90 sedimenting with a higher S-value (Lorenz et al., 2014). We did not observe any difference in complex formation of Cns1 with Hsp90 (Figure 3D), suggesting that the interaction is not affected by nucleotide-induced conformational changes. For stable complex formation with Hsp90, Cns1 requires the C-terminal MEEVD motif of Hsp90 (Figure 3E), confirming previous data (Hainzl et al., 2004; Tesic et al., 2003), and the TPR domain of Cns1 (Figures S3D–S3F).

Since the TPR domain and the N domain of Cns1 interact intramolecularly, we probed the potential competition of this interaction with the MEEVD peptide by NMR. We formed complexes between Cns1$^{1–82}$ and Cns1$^{70–205}$, in which one of the partners was $^{15}$N-labeled, and added the unlabeled MEEVD peptide. Strikingly, in the presence of the MEEVD peptide, some NMR signals of the N domain moved toward the position of the free Cns1$^{1–82}$ form, while in general the intensities of the signals in the N domain increased substantially. This indicates that the intramolecular interaction in Cns1 is disrupted by the MEEVD peptide (Figure S3G). The NMR spectral changes are most significant for residues involved in the helix comprising residues 67–70. In turn, the signals of the TPR domain showed extensive CSPs and line broadening upon peptide binding, especially in residues affected by the interaction with the N domain (Figure S3H). These results indicate a competitive interaction between the Cns1 N domain and the MEEVD motif to the TPR domain. In summary, binding of the Hsp90 MEEVD peptide releases weak contacts between the Cns1 TPR and N domain, suggesting a possible mechanism for regulating the interaction with Hsp90.

## Cns1 and Cpr7 Play a Role in Translation Elongation

Previous studies reported that Cns1 has an overlapping *in vivo* function with the Hsp90 co-chaperone Cpr7 (Dolinski et al., 1998; Marsh et al., 1998; Tesic et al., 2003). To test whether other Hsp90 co-chaperones are involved in the Cns1/Cpr7 pathway, we constructed double-mutant strains carrying either *cpr7*Δ or tet07-*CNS1* (doxycycline regulated promoter, leading to a knockdown of Cns1 in the presence of doxycycline) together with deletions or knockdowns of all known Hsp90 co-chaperones (Figures S4A–S4C). Interestingly, none of the co-chaperones additionally tested revealed a genetic interaction with *CNS1* and *CPR7*. Only the *cns1* and *cpr7* mutant strains exhibited a strong negative genetic interaction. We conclude that *CNS1* and *CPR7* form a unique epistasis module. Therefore, we focused our *in vivo* studies on the *cpr7* and *cns1* strains.

As expected, *cpr7*Δ cells showed a growth defect compared to the WT (Figure 4A). In the absence of doxycycline, i.e., Cns1 overexpression (Figure S4D), the tet07-*CNS1* mutant strain did not show a growth defect (Figure S4A). In the absence of doxycycline, the growth defect resulting from the deletion of the *cpr7* gene was abrogated, as *CNS1* is a multi-copy suppressor of *cpr7*Δ (Dolinski et al., 1998; Marsh et al., 1998). In the presence of doxycycline, the tet07-*CNS1* strain showed a strong growth defect. The double mutant was synthetic sick, as observed before (Tesic et al., 2003).

The *cns1* and *cpr7* mutant strains are known to be hypersensitive to the translation inhibitor hygromycin B (Albanèse et al., 2006; Tenge et al., 2015). Cns1 overexpression reverts this effect in the *cpr7*Δ strain (Figure 4A). To test whether the two co-chaperones are involved in protein translation, we monitored the incorporation of $^{35}$S-labeled methionine in proteins. We found that compared to the WT, protein translation was strongly diminished in *cpr7*Δ and tet07-*CNS1* knockdown cells and that this effect was even more pronounced in the double mutant (Figures 4B and S4E).

To determine which process is affected in the mutants, we used a polysome run-off assay (Ashe et al., 2000). Under normal translation conditions, 80S ribosomes form polysomes that can be chemically frozen by addition of cycloheximide (+CHX) (Figure 4C), thus preventing run-off. In contrast, glucose deprivation rapidly inhibits translation initiation and leads to polysome run-off from the mRNA. Strikingly, under glucose starvation conditions, polysome run-off was reduced in all three mutant strains as indicated by elevated polysome/monosome ratios (Figures 4C–4G). The strongest effect was observed in the tet07-*CNS1* *cpr7Δ* double mutant. Moreover, in the absence of doxycycline, polysome run-off was WT-like in the tet07-*CNS1* strain. Cns1 overexpression in the absence of doxycycline in the tet07-*CNS1* *cpr7*Δ strain reversed the polysome run-off defect of *cpr7*Δ (Figure S4F). These data strongly suggest that either translation elongation or termination is compromised. It is important to note that Cns1 sedimented with the light fractions,

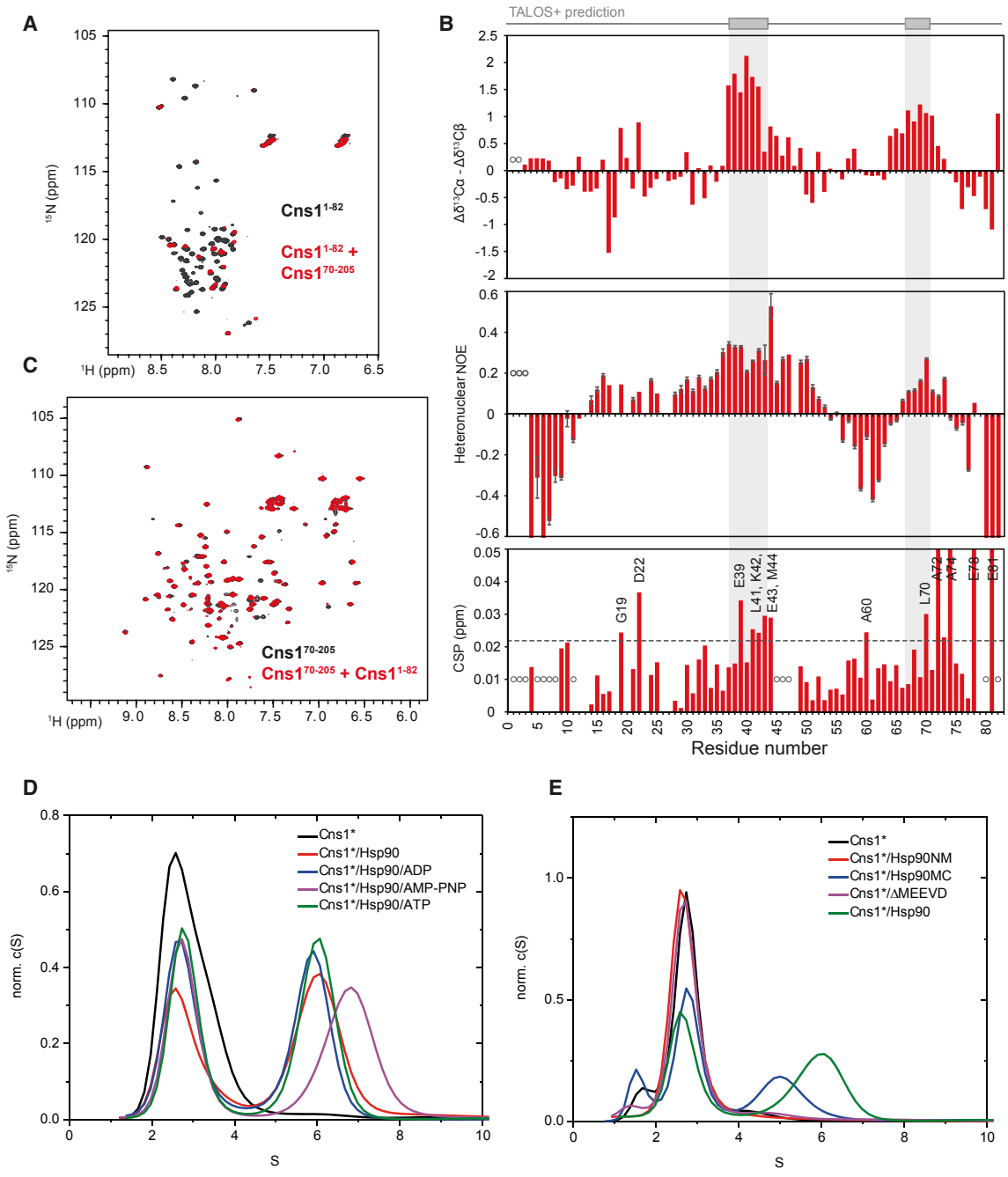


**Figure 3. Cns1 N Terminus Has Residual Structure and Interacts with TPR Domain**

(A) Superposition of $^{1}H$, $^{15}N$ HSQC spectra of the isolated N-terminal region of Cns1 ($Cns1^{1–82}$, black) free and in presence of 1.1 equivalents of unlabeled TPR domain ($Cns1^{70–205}$, red).

(B) Top: Secondary $^{13}C$ chemical shifts ($\delta^{13}C\alpha$-$\delta^{13}C\alpha_{ref}$) – ($\delta^{13}C\beta$-$\delta^{13}C\beta_{ref}$) of $Cns1^{1–82}$ (positive values indicate helical structure, zero corresponds to random coil). Secondary elements predicted by the program TALOS+ (Shen et al., 2009) are shown on top. Mid: Heteronuclear NOE values. Bottom: CSPs between $Cns1^{1–82}$ and $Cns1^{1–190}$, focusing on the 1–82 fragment. Residues that show perturbations above the median + standard deviation (dashed line) are annotated. In all plots, gray open circles correspond to residues without data.

(C) The same experiments as in (A) but this time with $^{15}N$-labeled TPR (black) and 1.1 equivalents of unlabeled N-terminal segment (red).

(D) Effect of the conformational state of Hsp90 on Cns1 binding analyzed by AUC sedimentation velocity experiments (500 nM Atto488-labeled Cns1, 10 μM Hsp90, and 2 mM nucleotides as indicated).

(E) Binding of Cns1 to different fragments of Hsp90 analyzed by AUC sedimentation velocity experiments (500 nM Atto488-labeled Cns1, 5 μM Hsp90 constructs as indicated).

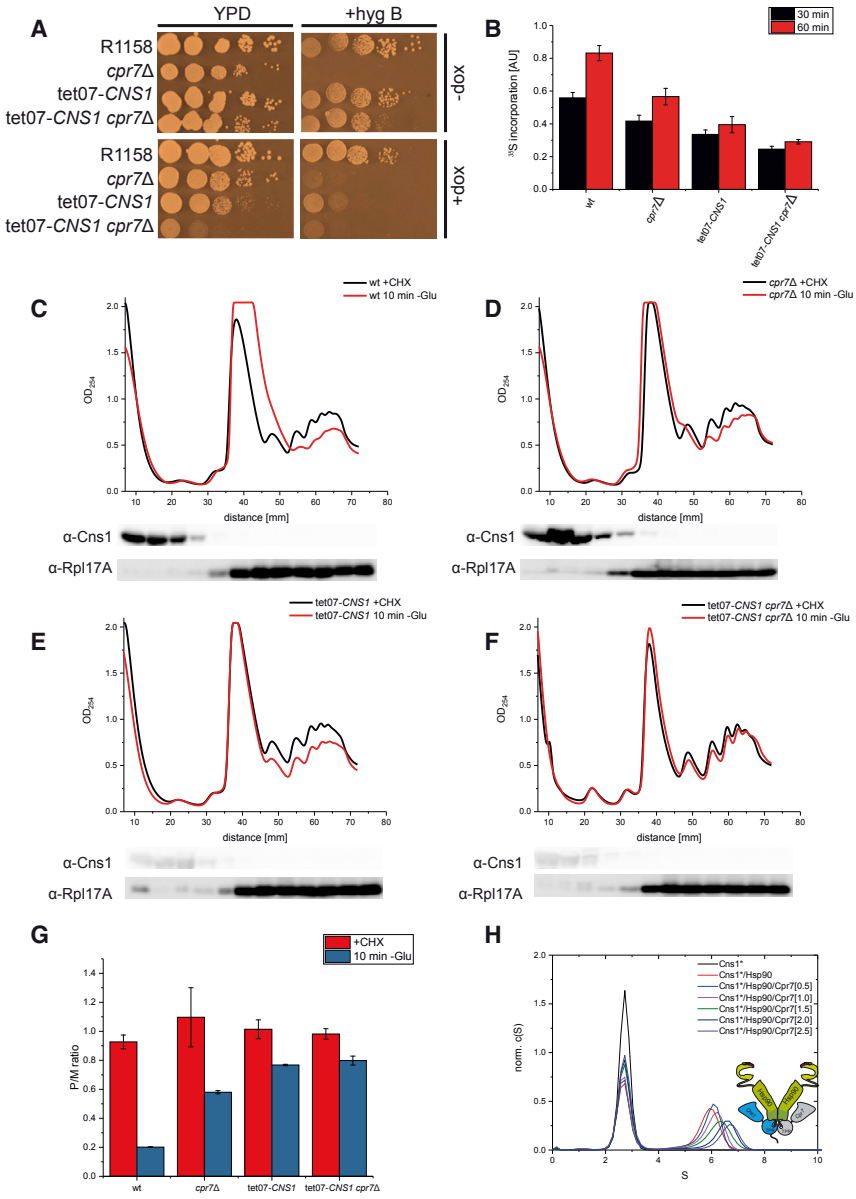


**Figure 4. Cns1 and Cpr7 Are Involved in Protein Translation**

(A) *cpr7Δ* and *cns1* knockdown mutants exhibit hygromycin B sensitivity. 10-fold serial dilutions of the indicated yeast strains were spotted onto YPD plates containing combinations of doxycycline (10 μg/mL) and hygromycin (25 μg/mL) as indicated. Plates were incubated at 30°C, and pictures were taken after 48 h. Representative pictures out of three biological replicates.

(B) Effect of the *cpr7Δ* and *cns1* knockdown mutants on protein synthesis. The indicated yeast cultures were supplemented with a mix of $^{35}$S-labeled methionine and cold methionine for 30 min and 60 min at 30°C, respectively. Total protein extracts were separated by SDS-PAGE. After autoradiography, signal intensities were quantified using ImageJ. Data from three independent biological replicates.

(C–F) Polysome run-off experiments using the wild-type (C), *cpr7Δ* (D), tet07-*CNS1* (E), and tet07-CNS1 *cpr7Δ* (F) strains. Cells were grown in YPD in the presence of 10 μg/mL doxycyclin and either treated with 100 μg/mL cycloheximide (CHX) or starved for 10 min in YP medium. Total cell extracts were run on 7%–47% sucrose gradients, and ribosome profiles were recorded at 254 nm. Western blot analysis of ribosome fractionations. Cns1 and Rpl17A were detected as indicated.

(G) Ratio of monosomes versus polysomes as shown in (C)–(F). Data from two independent biological replicates.

(H) Analysis of complex formation between Cns1, Hsp90, and Cpr7 by AUC sedimentation velocity experiments using 500 nM Atto488-labeled Cns1, 5 μM Hsp90, and Cpr7 as indicated. Normalized c(s) distributions were plotted against the apparent sedimentation coefficient (S).

indicating that its interaction with translating ribosomes is transient. As Cns1 and Cpr7 are able to form mixed complexes with Hsp90 (Figure 4H), they could act on the same client simultaneously.

## Cns1 Interacts Directly with Translation Factor eEF2 and the Recruiting Factor Hgh1

To define the physical interactome of Cns1, we performed tandem affinity purification with tagged Cns1 (Figure 5A). The readout on SDS-PAGE revealed the presence of Hsp90 and Hsp70. Intriguingly, we detected two additional proteins, which were identified as Hgh1 and eukaryotic elongation factor 2 (eEF2). The latter is encoded by two identical genes, *EFT1* and *EFT2*. The identity of a band at ~30 kDa could not be determined. For Hgh1, a specific function had not been defined yet. Our data suggest that Cns1, Hgh1, and eEF2 might be part of a protein complex that links the Hsp90 chaperone machine to protein translation. High-throughput studies support an interaction between Cns1 and Hgh1 (Gavin et al., 2002; Schlecht et al., 2012; Tarassov et al., 2008) and between Hgh1 and eEF2 (Krogan et al., 2004, 2006).

Analysis of the purified proteins by AUC showed that Cns1, besides binding to Hsp90, directly associates with eEF2 as well as with Hgh1 and that Hgh1 forms complexes with eEF2 and Cns1. Hgh1 does not bind Hsp90 (Figures 5B, 5C, and S5). This suggests a complex pattern of assembly in which Cns1 has 3 interaction partners and Hgh1 has 2. We also reconstituted the hetero-trimeric complex consisting of Cns1, Hgh1, and eEF2 and show that it can be joined by Hsp90, resulting in the quaternary Cns1-Hsp90-Hgh1-eEF2 assembly (Figures 5C and S5). Interestingly, the formation of this quaternary complex was strongly diminished when the inviable Cns1$^{51–385}$ construct was used, underlining the importance of the Cns1 N domain for association (Figure S5G).

H/DX experiments coupled to mass spectrometry allowed us to analyze regions in eEF2, Hgh1, and Cns1 affected by complex

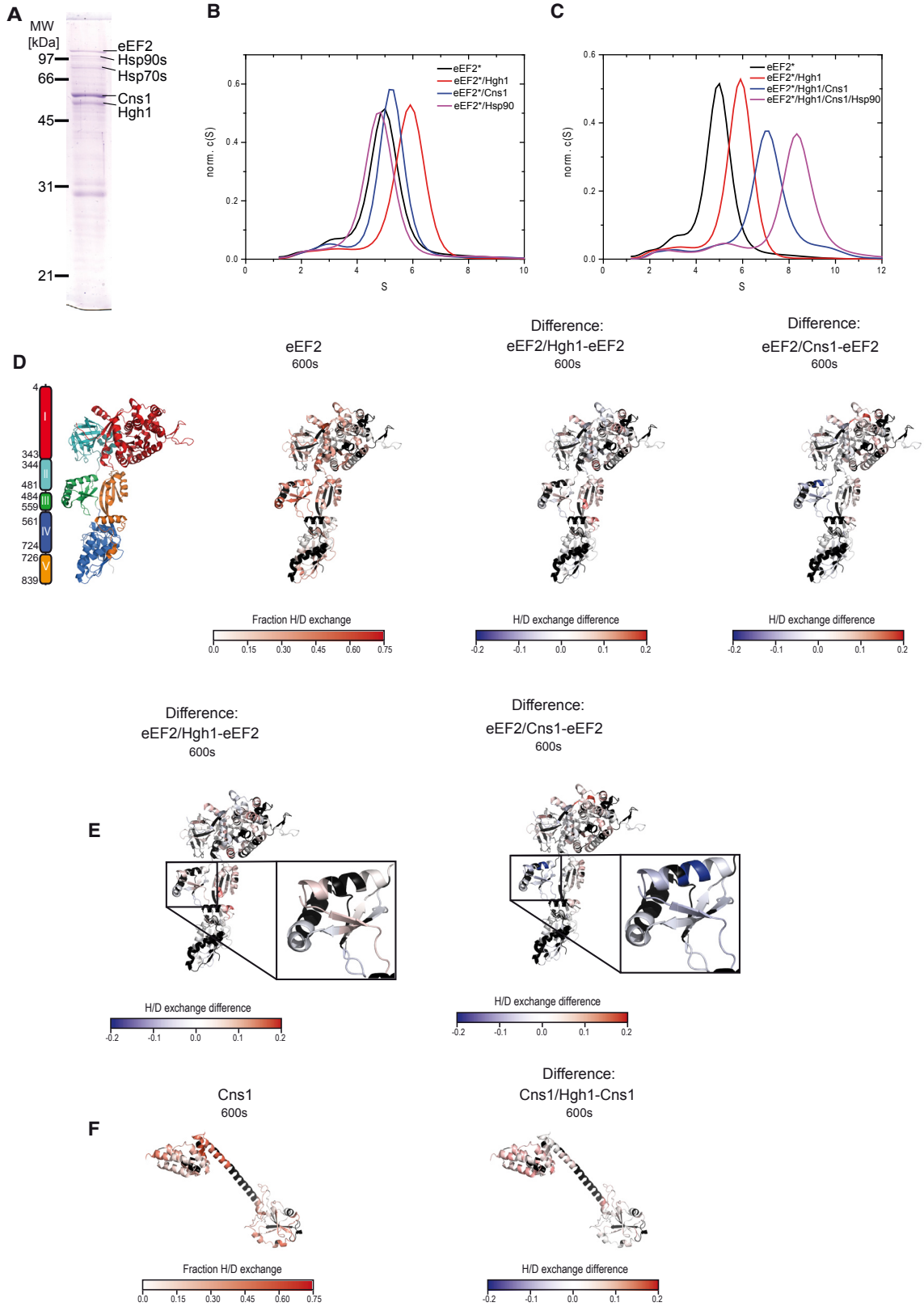


*(legend on next page)*

formation (Figures 5D–5F and S5H–S5K). In eEF2, we see changes in domain 1 and domain 3 upon binding of Cns1. Interestingly, for domain 3, which reveals the highest flexibility in eEF2 alone, we observe several segments that are stabilized against exchange in the presence of Cns1, suggesting that this domain constitutes the primary interaction site for Cns1 (Figure 5E).

When we analyzed the eEF2-Hgh1 complex, again domain 3 of eEF2 was affected. In this case, however, we see segments with higher or lower exchange compared to eEF2 alone, implicating that Hgh1 affects this domain in a complex manner. At early time points of exchange, the domain is more flexible than at later time points, which may indicate changes in its folding and stability triggered by the interaction with Hgh1 (Figure S5I).

For the Cns1-Hgh1 complex, it was possible to obtain information for both partners in the complex. The Cns1 TPR domain becomes more flexible in the presence of Hgh1 while the C domain remains largely unchanged. In the largely disordered N domain, no significant alterations were observed (Figures 5F and S5J). In Hgh1, regions with decreased exchange pointing toward sites of interaction were detected in the C domain, in the N domain, and also to some extent in the middle of the protein (Figure S5K).

AUC competition experiments suggest an interaction between Hgh1 and the C domain of Cns1. Interestingly, the complex is only disrupted completely when the TPR domain is also present (Figure S5L). Moreover, we could detect a weak interaction between the Cns1 N domain and Hgh1 by NMR (Figure S5M). In summary, this indicates that all three Cns1 domains are involved in the interaction with Hgh1.

### Cns1 Is Important for *In Vivo* Folding of eEF2

To test whether eEF2 is specifically affected by the Hsp90 components *in vivo*, we overexpressed proteins involved in translation elongation and termination. These are eEF1A, eEF2, eEF3, eIF5A, eRF3, and eRF1. Strikingly, only upon eEF2 overexpression, we observed a negative effect on the growth of *cpr7*Δ and *cns1* knockdown cells (Figures 6A and S6A). Cns1 overexpression in the *cpr7*Δ mutant reversed the eEF2 toxicity. Deletion of *HGH1* and *CPR7* led to an increased growth defect also observed in high-throughput studies (Costanzo et al., 2010, 2016; Kuzmin et al., 2018; Rizzolo et al., 2017, 2018). Again, Cns1 overexpression in the absence of doxycycline mitigated a negative genetic interaction between *hgh1*Δ and *cpr7*Δ. Interestingly, deletion of *HGH1* did not further enhance the growth defect of the tet07-*CNS1* strain in the presence of doxycycline, indicating that Cns1 is the limiting component in the Cns1-Hgh1 module (Figure S6B).

While the above results demonstrate the general importance of the chaperone components for eEF2 function, they do not report on their effects on eEF2 *in vivo*. To this end, we analyzed total eEF2 protein levels in different strains. We observed a strong decrease of eEF2 in the *cpr7*Δ, tet07-*CNS1*, and *hgh1*Δ strains (Figures 6B and S6C), suggesting that Cns1, Cpr7, and Hgh1 affect eEF2 folding and stability. To test this further, we analyzed the soluble versus insoluble fraction of eEF2. The experiments revealed that in the WT strain, eEF2 folded properly and was thus found in the supernatant. In contrast, eEF2 aggregated substantially in the absence of either Cns1 or Cpr7, and only ~20% of eEF2 was found in the supernatant (Figures 6B and S6C). In the *hgh1Δ* strain, ~40% remained soluble. Taken together, our experiments demonstrate that the *in vivo* folding and structural integrity of eEF2 depends strongly on Cns1, Cpr7, and Hgh1. As a control, we tested whether the knockout of *EFT2*, which depletes eEF2 levels to about 50%, also resulted in reduced protein translation (Figure S6D). Indeed, the mutant pheno-copied the *cns1*, *cpr7*, and *hgh1* mutants regarding $^{35}$S-methionine incorporation, providing further evidence that Cns1, Cpr7, and Hgh1 maintain protein translation via chaperoning of eEF2.

Finally, we tested to what extent the *de novo* folding of eEF2 depends on Hsp90. For this purpose, we treated WT yeast with the Hsp90 inhibitor Radicicol and then induced HA-eEF2 expression. Radiciol-treated cells showed a strong reduction of *de novo* synthesized eEF2, showing that Hsp90 has a pronounced impact on this process (Figure 6C). Together with the results on Cns1, Cpr7, and Hgh1, this demonstrates that all components of this complex affect eEF2 folding.

## DISCUSSION

Research on Hsp90 co-chaperones has shed light on their interaction with Hsp90 and their ability to modulate its chaperone

**Figure 5. Cns1 Directly Interacts with eEF2 and the Novel Adaptor Protein Hgh1**

(A) Tandem affinity purification of Cns1 indicates interaction of Cns1 with Hgh1 and eEF2 in addition to Hsp90 and Hsp70. Proteins were separated by SDS-PAGE and identified by mass spectrometry. The most prominent hits are indicated.

(B) eEF2 can directly bind Hgh1 and Cns1, but not Hsp90. AUC sedimentation velocity experiments using 500 nM Atto488-labeled eEF2 and all other indicated proteins at 2.5 μM. Normalized c(s) distributions were plotted against the apparent sedimentation coefficient (S).

(C) eEF2 is linked to Hsp90 via Hgh1 and Cns1. AUC sedimentation velocity experiments using 500 nM Atto488-labeled eEF2 and all other indicated proteins at 2.5 μM. Normalized c(s) distributions were plotted against the apparent sedimentation coefficient (S).

(D) Left: Domain structure of eEF2 according to InterPro. Numbers indicate first and last residue of the domain. Color code of the eEF2 domains mapped onto the crystal structure of yeast elongation factor 2 (PDB: 1N0U). Center-left: eEF2 is colored according to the fractional H/D exchange at time point 600 s. B values were mapped onto the crystal structure of yeast elongation factor 2. White to red coloring depicts an increase in deuteration. Black segments were not covered in H/D exchange experiments. For clarification, large helix in domain 4 is colored in black. Center-right: The difference in H/D exchange between the eEF2-Hgh1 complex versus eEF2 at 600 s. Blue colors correspond to lower and red colors to higher deuteration of the complex. Black segments were not covered. Right: Difference in H/D exchange between the eEF2-Cns1 complex and eEF2 after 600 s. Coloring same as in the center-right panel.

(E) Left: Difference in H/D exchange between the eEF2-Hgh1 complex and eEF2 after 600 s. Blue colors correspond to lower and red colors to higher deuteration of the complex. Black segments were not covered in H/D exchange experiments. Insert: Zoomed view into domain 3 of eEF2. Right: Difference in H/D exchange between the eEF2-Cns1 complex and eEF2 after 600 s. Coloring same as in left panel. Insert: Zoomed view into domain 3 of eEF2.

(F) Left: Fractional H/D exchange of Cns1 after 600 s mapped onto the crystal structure of Cns1$^{70–385}$ (PDB: 6HFT). White to red coloring depicts increase in deuteration. Black segments were not covered. Right: H/DX difference of Cns1 in complex with Hgh1 and Cns1 unbound. Color code same as in (E).

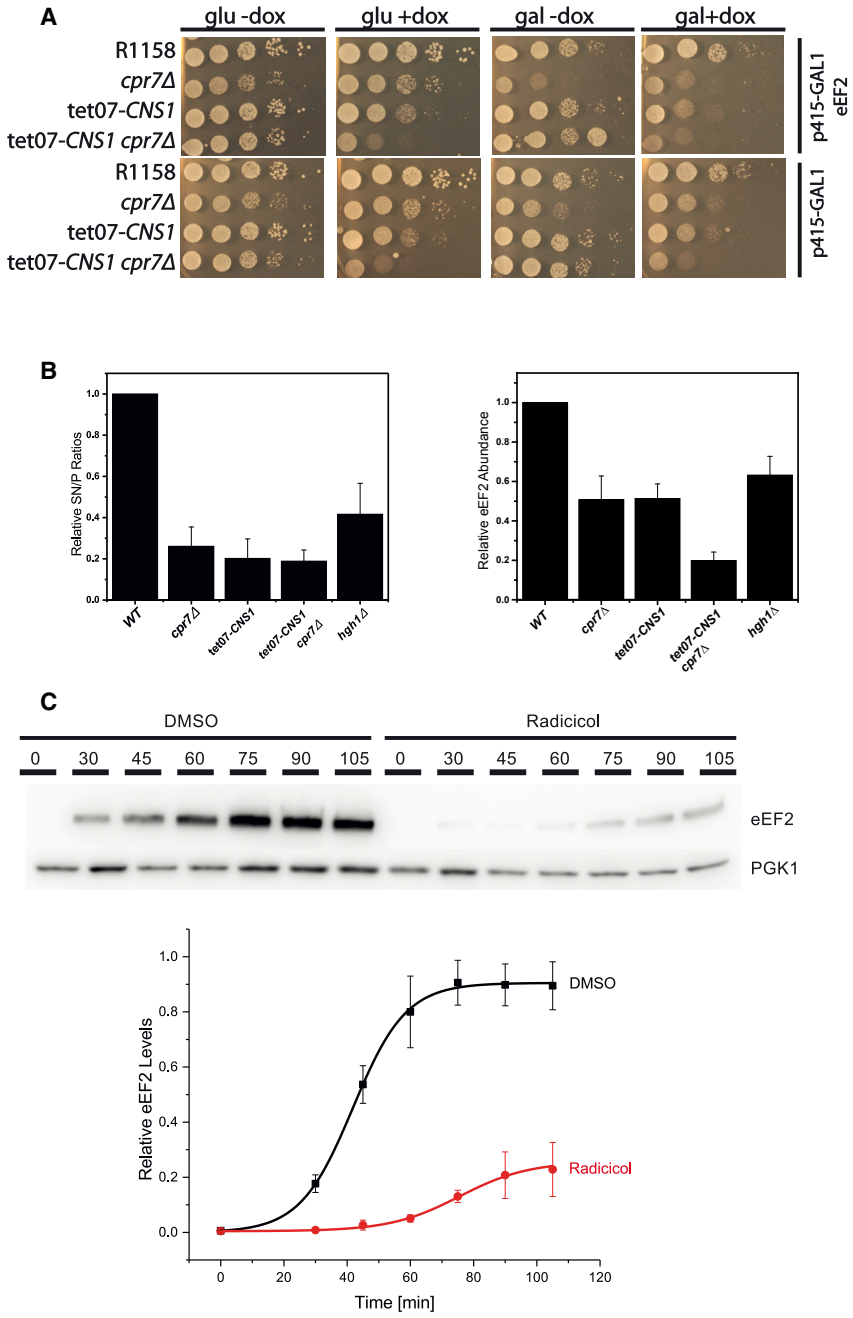


**Figure 6. Requirement of Cns1 and Hsp90 for eEF2 *De Novo* Folding**

(A) Overexpression of eEF2 is toxic for *cpr7Δ* cells. 10-fold serial dilutions of the indicated yeast strains were spotted onto glucose (glu)- or galactose (gal)-containing −Leu plates with or without 10 μg/mL doxycyclin (dox). eEF2 was overexpressed from the GAL1 promoter. Plates were incubated at 30°C, and pictures were taken after 48 h. Representative pictures out of 3 biological replicates.

(B) Cns1, Cpr7, and Hgh1 are crucial for folding of eEF2 *in vivo*. Lysates from the indicated yeast strains were separated into pellet and supernatant, and the distribution of eEF2 was analyzed by western blot. The ratio of eEF2 in the pellet fraction and total eEF2 levels were analyzed in the *tet07-CNS1*, *cpr7Δ*, tet07-*CNS1*/*cpr7Δ*, and *hgh1Δ* strains. Shown are the mean values and standard deviations from at least three independent biological replicates.

(C) eEF2 levels depend on Hsp90. *S. cerevisiae* was grown to log phase in the presence of the Hsp90 inhibitor Radicicol before the expression of HA-tagged eEF2 was induced by addition of D-galactose. Treatment with Radicicol entailed reduced levels of HA-EF2. The data represent means and standard deviations from 3 independent biological replicates.

cycle. Our study defines the structure of Cns1 and its role in *S. cerevisiae*. Strikingly, it links translation to Hsp90 control. Cns1 is important for the chaperoning of the translation elongation factor eEF2 in concert with Hsp90. For this function, we identified Hgh1 as an important co-factor.

Our structural analysis together with *in vivo* experiments established the fold of Cns1 and defined the parts essential for viability. We show that Cns1 is a "three-domain" protein. It contains two folded domains and an intrinsically disordered N domain. Interestingly, the C-terminal domain exhibits a novel fold, which is conserved between yeast Cns1 and human TTC4. Together with our *in vivo* complementation experiments, this strongly suggests that the function of Cns1 is conserved between yeast and man. Notably, the first segment with helical propensity revealed by NMR coincides with the region that conveys the essential function of Cns1 identified in our viability assay.

Several previous studies reported a functional overlap between Cns1 and Cpr7 *in vivo* (Marsh et al., 1998; Tenge et al., 2015; Tesic et al., 2003; Zuehlke and Johnson, 2012), but the nature of this genetic interaction was not clear. Moreover, both proteins were reported to weakly interact with the 80S ribosome (Albanèse et al., 2006; Tenge et al., 2015). Our analysis shows that overall translation is strongly compromised in *cns1* knockdown strains, reaching 50% of the normal levels. Furthermore, we identified translation elongation as the step being affected. Specifically, eEF2 was sensitive to *CNS1* depletion or *CPR7* deletion. In complexes isolated from cells, we detected, apart from Hsp90 and Hsp70, the proteins Hgh1 and eEF2. Hgh1 was an enigmatic protein whose structure and function were unknown. Only in high-throughput studies, an interaction between these factors had been suggested (Gavin et al., 2002; Schlecht et al., 2012; Tarassov et al., 2008). Interestingly, the analysis of the interaction of the purified proteins revealed a complex pattern: Cns1 can form complexes with eEF2 and Hgh1, in addition to its known interaction with

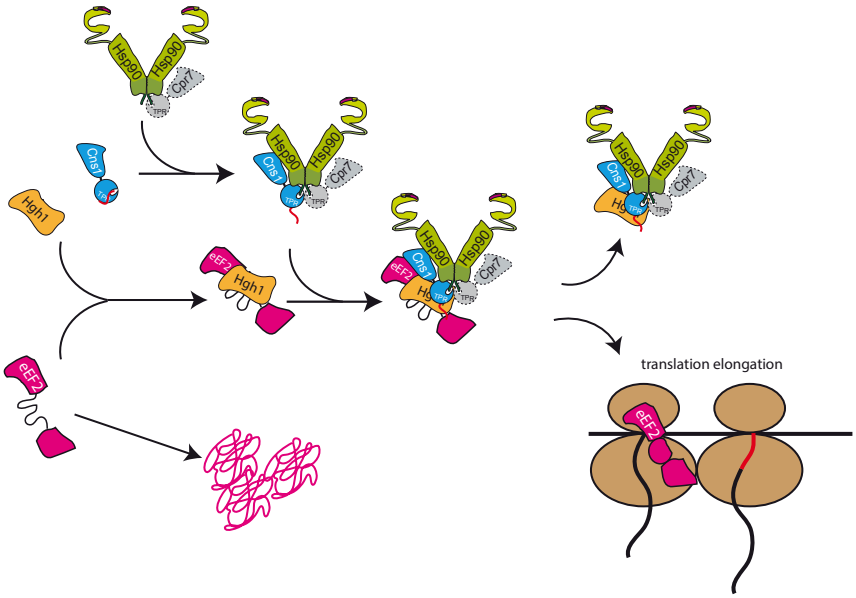


**Figure 7. Model of eEF2 Activation by Hgh1, Cns1, and Hsp90**

Hgh1 acts as an adaptor protein for both Cns1 and eEF2. Hsp90, Cns1, and Hgh1 form a multi-chaperone complex with eEF2. Cpr7 is involved in this process but may act on a parallel pathway. When folded properly, eEF2 can fulfill its role in translation elongation. In the absence of components of this complex, eEF2 is instable and forms aggregates in the cell.

Hsp90. In the binary Cns1-Hgh1 complex, both the C domain of Cns1 and its N-terminal part are important for a stable interaction. In this context, it is interesting to note that for survival of yeast cells, the C-terminal domain gains importance once the N-terminal segment is truncated. Together, this suggests an interplay in which the different parts of Cns1 fulfill synergistic functions. This becomes even more pronounced in the ternary complex with eEF2. Here, the N domain gains importance and undergoes additional interactions that stabilize the complex. Further complexity is added when Hsp90 is present. Binding of the MEEVD sequence of Hsp90 to the Cns1 TPR domain releases contacts between the N-terminal segments of Cns1 and its TPR domain. This may result in changes in the conformation of Cns1 and affect its interaction patterns. Our *in vivo* analysis revealed that all the components are involved in eEF2 folding. Specifically, the levels of newly synthesized eEF2 depend on Hsp90 and are strongly diminished in *cns1*, *cpr7*, and *hgh1* mutants. Besides, we could also show that eEF2 aggregated in *cns1*, *cpr7*, and *hgh1* mutant strains, which adds to the decreased levels and explains the observed translation defects. It is important to note that in our ribosome fractionation experiments, Cns1 sedimented with the light cytosolic fractions, indicating that it does not act as a co-factor of eEF2 during translation. Also, the low amounts of Cns1 per cell (Ghaemmaghami et al., 2003) point to a role in a specific process. Thus, taking the different pieces of evidence together, the most likely scenario is that the Hsp90 machinery is involved in the *de novo* folding of eEF2 after it leaves the ribosome. Interestingly, eEF2 overexpression affected growth in *cpr7* and *cns1* mutants. Presumably, the accumulation of misfolded eEF2 interferes with translation elongation. Indeed, it was reported previously that yeast cells keep their total eEF2 levels constant (Ortiz and Kinzy, 2005); interfering with the chaperones responsible for eEF2 folding might thus explain the observed phenotype. There are three possible explanations for the genetic interaction of *cns1* and *cpr7* mutants. First, Cns1 and Cpr7 show weak interaction with the ribosome. At least for Cns1, a stable interaction with the 80S ribosome is not essential, since it is mediated by the C-terminal Cns1 domain (Tenge et al., 2015), which is dispensable *in vivo*. Interestingly, Cns1 and Cpr7 were found in the same complex in a yeast strain lacking the C-terminal MEEVD motif of Hsp90, but they do not interact directly (Tesic et al., 2003). Thus, the two co-chaperones might find their *in vivo* target independently of Hsp90. Second, Cpr7 could be involved in processes upstream of or parallel to eEF2 folding which impair translation elongation and lead indirectly to eEF2 aggregation. This would explain the genetic interaction. Interestingly, *cpr7* mutants show a negative interaction with genes involved in the synthesis of diphtamid, which modifies His699 in eEF2 (Costanzo et al., 2010, 2016; Kuzmin et al., 2018). This modification is an example for a parallel or upstream pathway. Third, our *in vitro* approach might be missing an adaptor protein comparable to Hgh1 to stabilize or facilitate the interaction of Cpr7 with eEF2.

Our results put previous observations from high-throughput studies on connections between Hgh1, Cns1, eEF2, and Hsp90 (Alford and Brandman, 2018; Brandman et al., 2012; McClellan et al., 2007) into context. Interestingly, Hgh1 was also shown to be involved in stress granule formation (Cherkasov et al., 2015), a process that is connected to translation elongation. Our study now revealed that Cns1 and Hgh1 both directly interact with eEF2 and are crucial for its proper folding and activation *in vivo*. Importantly, these interactions are also conserved in human cells where TTC4 was reported to interact with human Hgh1, Hsp90, and human eEF2 (Crevel et al., 2008; Huttlin et al., 2017; Kristensen et al., 2012; Taipale et al., 2014). The CCT/TRiC chaperone system seems also to be involved in eEF2 folding, as human Hgh1 was reported to interact with CCT/TRiC (Hein et al., 2015), and yeast eEF2 is a client of CCT/TRiC (Rüßmann et al., 2012). Interestingly, Bracher, Hartl, and colleagues could show that Hgh1 acts as a recruiting factor for CCT/TRiC fostering the interaction of eEF2 with this chaperone complex (Mönkemeyer et al., 2019 [in this issue of *Molecular Cell*]). These findings suggest that Hgh1 recruits both the CCT/TRiC and the Hsp90 chaperone systems for eEF2 folding. Whether these chaperone machineries act in parallel or in a sequential manner remains to be seen.

In summary, we suggest a novel concept for the chaperone-dependent folding of eEF2 in yeast (Figure 7). Cns1 exhibits an

important bridging function as it interacts with eEF2, Hsp90, and Hgh1. The interactions of Cns1, Hgh1, and Hsp90 with eEF2 are required for its stability and solubility in yeast. In the absence of these factors, eEF2 aggregates and eEF2 levels decrease, leading to impaired translation elongation and loss of viability of yeast cells. The co-chaperone Cpr7 is also involved in these processes but may work by a different mechanism. The coordinated interaction of eEF2 with Cns1, Hgh1, and Hsp90 is required to chaperone eEF2 and support translation elongation, suggesting a complex regulatory process.

## STAR★METHODS

Detailed methods are provided in the online version of this paper and include the following:

- KEY RESOURCES TABLE
- CONTACT FOR REAGENT AND RESOURCE SHARING
- EXPERIMENTAL MODEL AND SUBJECT DETAILS
  - Yeast strains
- METHOD DETAILS
  - Protein purification
  - Protein fluorescent labeling
  - Tandem affinity purification
  - Protein identification by mass spectrometry
  - Crystallization and structure determination
  - NMR spectroscopy
  - Small Angle X-ray Scattering
  - Hydrogen/deuterium exchange (H/DX)
  - Analytical ultracentrifugation
  - Yeast mutant strain construction, 5′-FOA shuffling and spot assays
  - Ribosome fractionation, polysome run-off analysis, sample precipitation for western blot
  - $^{35}$S methionine labeling to quantify total protein translation in vivo
  - Analysis of eEF2 aggregation *in vivo*
  - Hsp90 inhibition in vivo
- QUANTIFICATION AND STATISTICAL ANALYSIS
- DATA AND SOFTWARE AVAILABILITY

## SUPPLEMENTAL INFORMATION

Supplemental Information can be found with this article online at https://doi.org/10.1016/j.molcel.2019.02.011.

## ACKNOWLEDGMENTS

This work was supported by grants from the DFG (SFB 1035 A3) to J.B. and M.S. and to M.G. (SFB1035 A2) and a fellowship from the IMPRS graduate school to F.H.S. E.M.H. acknowledges financial support by the Young Scholars' Program of the Bavarian Academy of Sciences and Humanities. M.M.B. was supported by a fellowship from the Fonds of the chemical industry. T.M. was supported by the Austrian Science Fund (FWF: P28854, I3792, and W1226 to T.M.), the Austrian Research Promotion Agency (FFG: 864690 and 870454), the Integrative Metabolism Research Center Graz, the Austrian infrastructure program 2016/2017, and BioTechMed/Graz. We thank Marcel Genge, Florian Ziegler, Florian Rührnößl, Gina Feind, and Astrid König for experimental support; Timm Hassemer and Ulrich Hartl for help with the ribosome fractionation; and Maximilian Reuter and Katja Sträßer for help with tandem affinity purification. We are grateful to Elke Deuerling for reagents; Dominik Maslak (Center for industrial Biotechnology TUM) for fermentation; Marina Rodnina, Frank Peske, and Namit Ranjan (MPI Göttingen) for discussions and experimental advice; and Dominic Helm and Bernhard Küster (TUM) for mass spec analysis. We thank the staff of the beamlines X06SA and X06DA at the Paul Scherrer Institute, Swiss Light Source, Villigen, Switzerland, and ID30B at the European Synchrotron Radiation Facility, Grenoble, France, for assistance during data collection.

## AUTHOR CONTRIBUTIONS

F.H.S., M.M.B., and C.D. performed *in vivo* and *in vitro* experiments. E.M.H. and M.G. determined the crystal structure and interpreted the data. D.A.R. and C.D. performed and analyzed AUC experiments. A.L. and M.S. performed NMR analysis. M.M. and F.H.S. carried out radioactive experiments. G.R. and T.M. performed SAXS analysis. F.H.S., E.M.H., M.G., A.L., M.S., T.M., and J.B. wrote the paper.

## DECLARATION OF INTERESTS

The authors declare no competing interests.

Received: September 13, 2018
Revised: December 17, 2018
Accepted: February 7, 2019
Published: March 12, 2019

## REFERENCES

Albanèse, V., Yam, A.Y., Baughman, J., Parnot, C., and Frydman, J. (2006). Systems analyses reveal two chaperone networks with distinct functions in eukaryotic cells. Cell *124*, 75–88.

Alford, B.D., and Brandman, O. (2018). Quantification of Hsp90 availability reveals differential coupling to the heat shock response. J. Cell Biol. *217*, 3809–3816.

Ali, M.M., Roe, S.M., Vaughan, C.K., Meyer, P., Panaretou, B., Piper, P.W., Prodromou, C., and Pearl, L.H. (2006). Crystal structure of an Hsp90-nucleotide-p23/Sba1 closed chaperone complex. Nature *440*, 1013–1017.

Ashe, M.P., De Long, S.K., and Sachs, A.B. (2000). Glucose depletion rapidly inhibits translation initiation in yeast. Mol. Biol. Cell *11*, 833–848.

Boczek, E.E., Reefschläger, L.G., Dehling, M., Struller, T.J., Häusler, E., Seidl, A., Kaila, V.R., and Buchner, J. (2015). Conformational processing of oncogenic v-Src kinase by the molecular chaperone Hsp90. Proc. Natl. Acad. Sci. USA *112*, E3189–E3198.

Brandman, O., Stewart-Ornstein, J., Wong, D., Larson, A., Williams, C.C., Li, G.W., Zhou, S., King, D., Shen, P.S., Weibezahn, J., et al. (2012). A ribosome-bound quality control complex triggers degradation of nascent peptides and signals translation stress. Cell *151*, 1042–1054.

Breslow, D.K., Cameron, D.M., Collins, S.R., Schuldiner, M., Stewart-Ornstein, J., Newman, H.W., Braun, S., Madhani, H.D., Krogan, N.J., and Weissman, J.S. (2008). A comprehensive strategy enabling high-resolution functional analysis of the yeast genome. Nat. Methods *5*, 711–718.

Brugge, J.S. (1986). Interaction of the Rous sarcoma virus protein pp60src with the cellular proteins pp50 and pp90. Curr. Top. Microbiol. Immunol. *123*, 1–22.

Catlett, M.G., and Kaplan, K.B. (2006). Sgt1p is a unique co-chaperone that acts as a client adaptor to link Hsp90 to Skp1p. J. Biol. Chem. *281*, 33739–33748.

Chen, V.B., Arendall, W.B., 3rd, Headd, J.J., Keedy, D.A., Immormino, R.M., Kapral, G.J., Murray, L.W., Richardson, J.S., and Richardson, D.C. (2010). MolProbity: all-atom structure validation for macromolecular crystallography. Acta Crystallogr. D Biol. Crystallogr. *66*, 12–21.

Cherkasov, V., Grousl, T., Theer, P., Vainshtein, Y., Glässer, C., Mongis, C., Kramer, G., Stoecklin, G., Knop, M., Mogk, A., and Bukau, B. (2015). Systemic control of protein synthesis through sequestration of translation

and ribosome biogenesis factors during severe heat stress. FEBS Lett. *589*, 3654–3664.

Choe, Y.J., Park, S.H., Hassemer, T., Körner, R., Vincenz-Donnelly, L., Hayer-Hartl, M., and Hartl, F.U. (2016). Failure of RQC machinery causes protein aggregation and proteotoxic stress. Nature *531*, 191–195.

Costanzo, M., Baryshnikova, A., Bellay, J., Kim, Y., Spear, E.D., Sevier, C.S., Ding, H., Koh, J.L., Toufighi, K., Mostafavi, S., et al. (2010). The genetic landscape of a cell. Science *327*, 425–431.

Costanzo, M., VanderSluis, B., Koch, E.N., Baryshnikova, A., Pons, C., Tan, G., Wang, W., Usaj, M., Hanchard, J., Lee, S.D., et al. (2016). A global genetic interaction network maps a wiring diagram of cellular function. Science *353*, aaf1420.

Crevel, G., Bennett, D., and Cotterill, S. (2008). The human TPR protein TTC4 is a putative Hsp90 co-chaperone which interacts with CDC6 and shows alterations in transformed cells. PLoS ONE *3*, e0001737.

Dolinski, K.J., Cardenas, M.E., and Heitman, J. (1998). CNS1 encodes an essential p60/Sti1 homolog in Saccharomyces cerevisiae that suppresses cyclophilin 40 mutations and interacts with Hsp90. Mol. Cell. Biol. *18*, 7344–7352.

Emsley, P., Lohkamp, B., Scott, W.G., and Cowtan, K. (2010). Features and development of Coot. Acta Crystallogr. D Biol. Crystallogr. *66*, 486–501.

Esposito, A.M., and Kinzy, T.G. (2014). In vivo [35 S]-methionine incorporation. In Methods in Enzymology, J. Lorsch, ed. (Academic Press), pp. 55–64.

Farrow, N.A., Muhandiram, R., Singer, A.U., Pascal, S.M., Kay, C.M., Gish, G., Shoelson, S.E., Pawson, T., Forman-Kay, J.D., and Kay, L.E. (1994a). Backbone dynamics of a free and phosphopeptide-complexed Src homology 2 domain studied by 15N NMR relaxation. Biochemistry *33*, 5984–6003.

Farrow, N.A., Zhang, O., Forman-Kay, J.D., and Kay, L.E. (1994b). A heteronuclear correlation experiment for simultaneous determination of 15N longitudinal decay and chemical exchange rates of systems in slow equilibrium. J. Biomol. NMR *4*, 727–734.

Franke, D., and Svergun, D.I. (2009). *DAMMIF*, a program for rapid *ab-initio* shape determination in small-angle scattering. J. Appl. Cryst. *42*, 342–346.

Gavin, A.C., Bösche, M., Krause, R., Grandi, P., Marzioch, M., Bauer, A., Schultz, J., Rick, J.M., Michon, A.M., Cruciat, C.M., et al. (2002). Functional organization of the yeast proteome by systematic analysis of protein complexes. Nature *415*, 141–147.

Ghaemmaghami, S., Huh, W.K., Bower, K., Howson, R.W., Belle, A., Dephoure, N., O'Shea, E.K., and Weissman, J.S. (2003). Global analysis of protein expression in yeast. Nature *425*, 737–741.

Gietz, R.D., and Woods, R.A. (2002). Transformation of yeast by lithium acetate/single-stranded carrier DNA/polyethylene glycol method. Methods Enzymol. *350*, 87–96.

Hainzl, O., Wegele, H., Richter, K., and Buchner, J. (2004). Cns1 is an activator of the Ssa1 ATPase activity. J. Biol. Chem. *279*, 23267–23273.

Hein, M.Y., Hubner, N.C., Poser, I., Cox, J., Nagaraj, N., Toyoda, Y., Gak, I.A., Weisswange, I., Mansfeld, J., Buchholz, F., et al. (2015). A human interactome in three quantitative dimensions organized by stoichiometries and abundances. Cell *163*, 712–723.

Hessling, M., Richter, K., and Buchner, J. (2009). Dissection of the ATP-induced conformational cycle of the molecular chaperone Hsp90. Nat. Struct. Mol. Biol. *16*, 287–293.

Holm, L., and Rosenström, P. (2010). Dali server: conservation mapping in 3D. Nucleic Acids Res. *38*, W545–W549.

Huttlin, E.L., Bruckner, R.J., Paulo, J.A., Cannon, J.R., Ting, L., Baltier, K., Colby, G., Gebreab, F., Gygi, M.P., Parzen, H., et al. (2017). Architecture of the human interactome defines protein communities and disease networks. Nature *545*, 505–509.

Janke, C., Magiera, M.M., Rathfelder, N., Taxis, C., Reber, S., Maekawa, H., Moreno-Borchart, A., Doenges, G., Schwob, E., Schiebel, E., and Knop, M. (2004). A versatile toolbox for PCR-based tagging of yeast genes: new fluorescent proteins, more markers and promoter substitution cassettes. Yeast *21*, 947–962.

Johnson, J.L. (2012). Evolution and function of diverse Hsp90 homologs and cochaperone proteins. Biochim. Biophys. Acta *1823*, 607–613.

Johnson, B.D., Schumacher, R.J., Ross, E.D., and Toft, D.O. (1998). Hop modulates Hsp70/Hsp90 interactions in protein folding. J. Biol. Chem. *273*, 3679–3686.

Kabsch, W. (2010). XDS. Acta Crystallogr D Biol Crystallogr *66*, 125–132.

Kachroo, A.H., Laurent, J.M., Yellman, C.M., Meyer, A.G., Wilke, C.O., and Marcotte, E.M. (2015). Evolution. Systematic humanization of yeast genes reveals conserved functions and genetic modularity. Science *348*, 921–925.

Kitagawa, K., Skowyra, D., Elledge, S.J., Harper, J.W., and Hieter, P. (1999). SGT1 encodes an essential component of the yeast kinetochore assembly pathway and a novel subunit of the SCF ubiquitin ligase complex. Mol. Cell *4*, 21–33.

Kristensen, A.R., Gsponer, J., and Foster, L.J. (2012). A high-throughput approach for measuring temporal changes in the interactome. Nat. Methods *9*, 907–909.

Krogan, N.J., Peng, W.T., Cagney, G., Robinson, M.D., Haw, R., Zhong, G., Guo, X., Zhang, X., Canadien, V., Richards, D.P., et al. (2004). High-definition macromolecular composition of yeast RNA-processing complexes. Mol. Cell *13*, 225–239.

Krogan, N.J., Cagney, G., Yu, H., Zhong, G., Guo, X., Ignatchenko, A., Li, J., Pu, S., Datta, N., Tikuisis, A.P., et al. (2006). Global landscape of protein complexes in the yeast Saccharomyces cerevisiae. Nature *440*, 637–643.

Kushnirov, V.V. (2000). Rapid and reliable protein extraction from yeast. Yeast *16*, 857–860.

Kuzmin, E., VanderSluis, B., Wang, W., Tan, G., Deshpande, R., Chen, Y., Usaj, M., Balint, A., Mattiazzi Usaj, M., van Leeuwen, J., et al. (2018). Systematic analysis of complex genetic interactions. Science *360*, eaao1729.

Laskowski, R.A., Moss, D.S., and Thornton, J.M. (1993). Main-chain bond lengths and bond angles in protein structures. J. Mol. Biol. *231*, 1049–1067.

Li, J., Richter, K., and Buchner, J. (2011). Mixed Hsp90-cochaperone complexes are important for the progression of the reaction cycle. Nat. Struct. Mol. Biol. *18*, 61–66.

Lorenz, O.R., Freiburger, L., Rutz, D.A., Krause, M., Zierer, B.K., Alvira, S., Cuéllar, J., Valpuesta, J.M., Madl, T., Sattler, M., and Buchner, J. (2014). Modulation of the Hsp90 chaperone cycle by a stringent client protein. Mol. Cell *53*, 941–953.

Marsh, J.A., Kalton, H.M., and Gaber, R.F. (1998). Cns1 is an essential protein associated with the hsp90 chaperone complex in Saccharomyces cerevisiae that can restore cyclophilin 40-dependent functions in cpr7Delta cells. Mol. Cell. Biol. *18*, 7353–7359.

Mayer, M.P., and Le Breton, L. (2015). Hsp90: breaking the symmetry. Mol. Cell *58*, 8–20.

McClellan, A.J., Xia, Y., Deutschbauer, A.M., Davis, R.W., Gerstein, M., and Frydman, J. (2007). Diverse cellular functions of the Hsp90 molecular chaperone uncovered using systems approaches. Cell *131*, 121–135.

McCoy, A.J., Grosse-Kunstleve, R.W., Adams, P.D., Winn, M.D., Storoni, L.C., and Read, R.J. (2007). Phaser crystallographic software. J. Appl. Cryst. *40*, 658–674.

Mönkemeyer, L., Klaips, C.L., Balchin, D., Körner, R., Hartl, F.U., and Bracher, A. (2019). Chaperone function of Hgh1 in the biogenesis of eukaryotic elongation factor 2. Mol. Cell *74*. Published online March 12, 2019. https://doi.org/10.1016/j.molcel.2019.01.034.

Nathan, D.F., Vos, M.H., and Lindquist, S. (1999). Identification of SSF1, CNS1, and HCH1 as multicopy suppressors of a Saccharomyces cerevisiae Hsp90 loss-of-function mutation. Proc. Natl. Acad. Sci. USA *96*, 1409–1414.

Nesvizhskii, A.I., Keller, A., Kolker, E., and Aebersold, R. (2003). A statistical model for identifying proteins by tandem mass spectrometry. Anal. Chem. *75*, 4646–4658.

Ortiz, P.A., and Kinzy, T.G. (2005). Dominant-negative mutant phenotypes and the regulation of translation elongation factor 2 levels in yeast. Nucleic Acids Res. *33*, 5740–5748.

Ortiz, P.A., Ulloque, R., Kihara, G.K., Zheng, H., and Kinzy, T.G. (2006). Translation elongation factor 2 anticodon mimicry domain mutants affect fidelity and diphtheria toxin resistance. J. Biol. Chem. *281*, 32639–32648.

Pal, M., Morgan, M., Phelps, S.E., Roe, S.M., Parry-Morris, S., Downs, J.A., Polier, S., Pearl, L.H., and Prodromou, C. (2014). Structural basis for phosphorylation-dependent recruitment of Tel2 to Hsp90 by Pih1. Structure *22*, 805–818.

Panaretou, B., Prodromou, C., Roe, S.M., O'Brien, R., Ladbury, J.E., Piper, P.W., and Pearl, L.H. (1998). ATP binding and hydrolysis are essential to the function of the Hsp90 molecular chaperone in vivo. EMBO J. *17*, 4829–4836.

Panaretou, B., Siligardi, G., Meyer, P., Maloney, A., Sullivan, J.K., Singh, S., Millson, S.H., Clarke, P.A., Naaby-Hansen, S., Stein, R., et al. (2002). Activation of the ATPase activity of hsp90 by the stress-regulated cochaperone aha1. Mol. Cell *10*, 1307–1318.

Pannu, N.S., Waterreus, W.J., Skubák, P., Sikharulidze, I., Abrahams, J.P., and de Graaff, R.A. (2011). Recent advances in the CRANK software suite for experimental phasing. Acta Crystallogr. D Biol. Crystallogr. *67*, 331–337.

Perrakis, A., Sixma, T.K., Wilson, K.S., and Lamzin, V.S. (1997). wARP: improvement and extension of crystallographic phases by weighted averaging of multiple-refined dummy atomic models. Acta Crystallogr. D Biol. Crystallogr. *53*, 448–455.

Petoukhov, M.V., and Svergun, D.I. (2005). Global rigid body modeling of macromolecular complexes against small-angle scattering data. Biophys J. *89*, 1237–1250.

Petoukhov, M.V., Franke, D., Shkumatov, A.V., Tria, G., Kikhney, A.G., Gajda, M., Gorba, C., Mertens, H.D., Konarev, P.V., and Svergun, D.I. (2012). New developments in the *ATSAS* program package for small-angle scattering data analysis. J. Appl. Cryst. *45*, 342–350.

Puig, O., Caspary, F., Rigaut, G., Rutz, B., Bouveret, E., Bragado-Nilsson, E., Wilm, M., and Séraphin, B. (2001). The tandem affinity purification (TAP) method: a general procedure of protein complex purification. Methods *24*, 218–229.

Retzlaff, M., Hagn, F., Mitschke, L., Hessling, M., Gugel, F., Kessler, H., Richter, K., and Buchner, J. (2010). Asymmetric activation of the hsp90 dimer by its cochaperone aha1. Mol. Cell *37*, 344–354.

Richter, K., Muschler, P., Hainzl, O., and Buchner, J. (2001). Coordinated ATP hydrolysis by the Hsp90 dimer. J. Biol. Chem. *276*, 33689–33696.

Richter, K., Muschler, P., Hainzl, O., Reinstein, J., and Buchner, J. (2003). Sti1 is a non-competitive inhibitor of the Hsp90 ATPase. Binding prevents the N-terminal dimerization reaction during the atpase cycle. J. Biol. Chem. *278*, 10328–10333.

Rizzolo, K., Huen, J., Kumar, A., Phanse, S., Vlasblom, J., Kakihara, Y., Zeineddine, H.A., Minic, Z., Snider, J., Wang, W., et al. (2017). Features of the chaperone cellular network revealed through systematic interaction mapping. Cell Rep. *20*, 2735–2748.

Rizzolo, K., Kumar, A., Kakihara, Y., Phanse, S., Minic, Z., Snider, J., Stagljar, I., Zilles, S., Babu, M., and Houry, W.A. (2018). Systems analysis of the genetic interaction network of yeast molecular chaperones. Mol Omics *14*, 82–94.

Rosam, M., Krader, D., Nickels, C., Hochmair, J., Back, K.C., Agam, G., Barth, A., Zeymer, C., Hendrix, J., Schneider, M., et al. (2018). Bap (Sil1) regulates the molecular chaperone BiP by coupling release of nucleotide and substrate. Nat. Struct. Mol. Biol. *25*, 90–100.

Russell, L.C., Whitt, S.R., Chen, M.S., and Chinkers, M. (1999). Identification of conserved residues required for the binding of a tetratricopeptide repeat domain to heat shock protein 90. J. Biol. Chem. *274*, 20060–20063.

Rüßmann, F., Stemp, M.J., Mönkemeyer, L., Etchells, S.A., Bracher, A., and Hartl, F.U. (2012). Folding of large multidomain proteins by partial encapsulation in the chaperonin TRiC/CCT. Proc. Natl. Acad. Sci. USA *109*, 21208–21215.

Sattler, M., Schleucher, J., and Griesinger, C. (1999). A novel NMR experiment for the sequential assignment of proline residues and proline stretches in 13C/15N labeled proteins. J. Biomol. NMR *13*, 381–385.

Scheufler, C., Brinker, A., Bourenkov, G., Pegoraro, S., Moroder, L., Bartunik, H., Hartl, F.U., and Moarefi, I. (2000). Structure of TPR domain-peptide complexes: critical elements in the assembly of the Hsp70-Hsp90 multichaperone machine. Cell *101*, 199–210.

Schlecht, U., Miranda, M., Suresh, S., Davis, R.W., and St Onge, R.P. (2012). Multiplex assay for condition-dependent changes in protein-protein interactions. Proc. Natl. Acad. Sci. USA *109*, 9213–9218.

Schmid, A.B., Lagleder, S., Gräwert, M.A., Röhl, A., Hagn, F., Wandinger, S.K., Cox, M.B., Demmer, O., Richter, K., Groll, M., et al. (2012). The architecture of functional modules in the Hsp90 co-chaperone Sti1/Hop. EMBO J. *31*, 1506–1517.

Schopf, F.H., Biebl, M.M., and Buchner, J. (2017). The HSP90 chaperone machinery. Nat. Rev. Mol. Cell Biol. *18*, 345–360.

Schuck, P. (2000). Size-distribution analysis of macromolecules by sedimentation velocity ultracentrifugation and lamm equation modeling. Biophys. J. *78*, 1606–1619.

Semenyuk, A.V., and Svergun, D.I. (1991). GNOM– a program package for small-angle scattering data processing. J. Appl. Crystallogr. *24*, 537–540.

Shen, Y., Delaglio, F., Cornilescu, G., and Bax, A. (2009). TALOS+: a hybrid method for predicting protein backbone torsion angles from NMR chemical shifts. J. Biomol. NMR *44*, 213–223.

Shevchenko, A., Tomas, H., Havlis, J., Olsen, J.V., and Mann, M. (2006). In-gel digestion for mass spectrometric characterization of proteins and proteomes. Nat. Protoc. *1*, 2856–2860.

Shiau, A.K., Harris, S.F., Southworth, D.R., and Agard, D.A. (2006). Structural Analysis of E. coli hsp90 reveals dramatic nucleotide-dependent conformational rearrangements. Cell *127*, 329–340.

Sinars, C.R., Cheung-Flynn, J., Rimerman, R.A., Scammell, J.G., Smith, D.F., and Clardy, J. (2003). Structure of the large FK506-binding protein FKBP51, an Hsp90-binding protein and a component of steroid receptor complexes. Proc. Natl. Acad. Sci. USA *100*, 868–873.

Stanitzek, S. (2005). Structural characterization of PPC-synthetase from the biosynthesis of coenzyme A; X-ray structure of the co-chaperone Cns1 218-C and the deglycosylated Fc-fragment of the antibody MAK33 from mice. Dissertation (Technische Universität München).

Svergun, D., Barberato, C., and Koch, M.H.J. (1995). CRYSOL—a program to evaluate X-ray solution scattering of biological macromolecules from atomic coordinates. J. Appl. Crystallogr. *28*, 768–773.

Taipale, M., Tucker, G., Peng, J., Krykbaeva, I., Lin, Z.Y., Larsen, B., Choi, H., Berger, B., Gingras, A.C., and Lindquist, S. (2014). A quantitative chaperone interaction network reveals the architecture of cellular protein homeostasis pathways. Cell *158*, 434–448.

Tarassov, K., Messier, V., Landry, C.R., Radinovic, S., Serna Molina, M.M., Shames, I., Malitskaya, Y., Vogel, J., Bussey, H., and Michnick, S.W. (2008). An in vivo map of the yeast protein interactome. Science *320*, 1465–1470.

Tenge, V.R., Zuehlke, A.D., Shrestha, N., and Johnson, J.L. (2015). The Hsp90 cochaperones Cpr6, Cpr7, and Cns1 interact with the intact ribosome. Eukaryot. Cell *14*, 55–63.

Tesic, M., Marsh, J.A., Cullinan, S.B., and Gaber, R.F. (2003). Functional interactions between Hsp90 and the co-chaperones Cns1 and Cpr7 in Saccharomyces cerevisiae. J. Biol. Chem. *278*, 32692–32701.

Tong, A.H.Y., and Boone, C. (2007). 16 high-throughput strain construction and systematic synthetic lethal screening in Saccharomycescerevisiae. In Methods in Microbiology, I. Stansfield and M.J.R. Stark, eds. (Academic Press), pp. 369–707.

Vagin, A.A., Steiner, R.A., Lebedev, A.A., Potterton, L., McNicholas, S., Long, F., and Murshudov, G.N. (2004). REFMAC5 dictionary: organization of prior chemical knowledge and guidelines for its use. Acta Crystallogr. Sect. D Biol. Crystallogr. *60*, 2184–2195.

Volkov, V.V., and Svergun, D.I. (2003). Uniqueness of ab initio shape determination in small-angle scattering. J. Appl. Crystallogr. *36*, 860–864.

Vranken, W.F., Boucher, W., Stevens, T.J., Fogh, R.H., Pajon, A., Llinas, M., Ulrich, E.L., Markley, J.L., Ionides, J., and Laue, E.D. (2005). The CCPN data model for NMR spectroscopy: development of a software pipeline. Proteins *59*, 687–696.

Wishart, D.S., and Sykes, B.D. (1994). The 13C chemical-shift index: a simple method for the identification of protein secondary structure using 13C chemical-shift data. J. Biomol. NMR *4*, 171–180.

Zuehlke, A.D., and Johnson, J.L. (2012). Chaperoning the chaperone: a role for the co-chaperone Cpr7 in modulating Hsp90 function in Saccharomyces cerevisiae. Genetics *191*, 805–814.

# STAR★METHODS

## KEY RESOURCES TABLE

| REAGENT or RESOURCE | SOURCE | IDENTIFIER |
|---|---|---|
| Antibodies | | |
| Rabbit polyclonal anti-Cns1 | Pineda, Berlin | N/A |
| Rabbit polyclonal anti-eEF2 | Kerafast, Boston | Cat# ED7002 |
| Mouse monoclonal anti-PGK1 | Invitrogen | Cat# PAS-286212 |
| Anti-rabbit-Antibody | Sigma-Aldrich | Cat# A0545; RRID: AB_257896 |
| Anti-mouse-Antibody | Sigma-Aldrich | Cat# A4789; RRID: AB_258201 |
| Rabbit polyclonal anti-Rpl17A | E. Deuerling | N/A |
| Chemicals, Peptides, and Recombinant Proteins | | |
| Doxycyclin | Sigma-Aldrich | Cat# D1822 |
| Hygromycin B | Sigma-Aldrich | Cat# 10843555001 Roche |
| 5′-Fuoroorotic acid | Thermo-Fisher Scientific | Cat# R0812 |
| $^{35}$S methionine | Hartmann Analytics | Cat# KSM-01 |
| Radicicol | Sigma-Aldrich | Cat# R2146 |
| ATP | Roche | Cat# 1059987001 |
| AMP-PNP | Sigma-Aldrich | Cat# 10102547001 Roche |
| ADP | Sigma-Aldrich | Cat# 01905 |
| Deposited Data | | |
| Cns1$^{221–385}$ | PDB | PDB: 6HFM |
| TTC4$^{217–387}$ | PDB | PDB: 6HFO |
| Cns1$^{70–385}$ | PDB | PDB: 6HFT |
| Experimental Models: Organisms/Strains | | |
| *hgh1Δ* R1158 hgh1::hygNT1 | This study | N/A |
| *hgh1Δ* cpr7Δ R1158 hgh1::hygNT1 cpr7::natNT2 | This study | N/A |
| *hgh1Δ* tet07-CNS1 R1158 pCNS1::kanR-tet07-TATA hgh1::hygNT1 | This study | N/A |
| *hgh1Δ* cpr7Δ tet07-CNS1 R1158 pCNS1::kanR-tet07-TATA cpr7::natNT2 hgh1::hygNT1 | This study | N/A |
| *eft2Δ* BY4741; MATa; ura3Δ0; leu2Δ0; his3Δ1; met15Δ0; YDR385w::kanMX4 | Euroscarf | Cat# Y04221 |
| Cns1-TAP BY4741; MATa; ura3Δ0; leu2Δ0; his3Δ1; met15Δ0; pCNS1-TAP::HisMX6 | Dharmacon | Cat# YSC1178 |
| *cns1Δ* [CNS1] BY4741 MATa; ura3Δ0; leu2Δ0; his3Δ1; met15Δ0; [p426-GPD-CNS1$^{wt}$] | L. Mitschke | N/A |
| *sti1Δ cpr7Δ* Y8205 MATa can1::STE2pr-Sp-his5 lyp1::STE3pr-Sp-LEU2 his3-1 leu2-0 cpr7::natMX sti1::kanMX4 | This study | N/A |
| *tah1Δ cpr7Δ* Y8205 MATa can1::STE2pr-Sp-his5 lyp1::STE3pr-Sp-LEU2 his3-1 leu2-0 cpr7::natMX tah1::kanMX4 | This study | N/A |
| *pih1Δ cpr7Δ* Y8205 MATa can1::STE2pr-Sp-his5 lyp1::STE3pr-Sp-LEU2 his3-1 leu2-0 cpr7::natMX pih1::kanMX4 | This study | N/A |
| *cpr6Δ cpr7Δ* Y8205 MATa can1::STE2pr-Sp-his5 lyp1::STE3pr-Sp-LEU2 his3-1 leu2-0 cpr7::natMX cpr6::kanMX4 | This study | N/A |
| *aha1Δ cpr7Δ* Y8205 MATa can1::STE2pr-Sp-his5 lyp1::STE3pr-Sp-LEU2 his3-1 leu2-0 cpr7::natMX aha1::kanMX4 | This study | N/A |
| *hch1Δ cpr7Δ* Y8205 MATa can1::STE2pr-Sp-his5 lyp1::STE3pr-Sp-LEU2 his3-1 leu2-0 cpr7::natMX hch1::kanMX4 | This study | N/A |
| *ppt1Δ cpr7Δ* Y8205 MATa can1::STE2pr-Sp-his5 lyp1::STE3pr-Sp-LEU2 his3-1 leu2-0 cpr7::natMX ppt1::kanMX4 | This study | N/A |

(*Continued on next page*)

***Continued***

| REAGENT or RESOURCE | SOURCE | IDENTIFIER |
|---|---|---|
| *sba1Δ cpr7Δ* Y8205 MATa can1::STE2pr-Sp-his5 lyp1::STE3pr-Sp-LEU2 his3-1 leu2-0 cpr7::natMX sba1::kanMX4 | This study | N/A |
| *cns1-DAmP cpr7Δ* Y8205 MATa can1::STE2pr-Sp-his5 lyp1::STE3pr-Sp-LEU2 his3-1 leu2-0 cpr7::natMX cns1-DAmP::kanMX4 | This study | N/A |
| *cdc371-DAmP cpr7Δ* Y8205 MATa can1::STE2pr-Sp-his5 lyp1::STE3pr-Sp-LEU2 his3-1 leu2-0 cpr7::natMX cdc37-DAmP::kanMX4 | This study | N/A |
| *sti1Δ* tet07-CNS1 Y8205 MATa can1::STE2pr-Sp-his5 lyp1::STE3pr-Sp-LEU2 his3-1 leu2-0 URA3::CMV-tTA pCNS1::natMX-tet07-TATA sti1::kanMX4 | This study | N/A |
| *tah1Δ* tet07-CNS1 Y8205 MATa can1::STE2pr-Sp-his5 lyp1::STE3pr-Sp-LEU2 his3-1 leu2-0 URA3::CMV-tTA pCNS1::natMX-tet07-TATA tah1::kanMX4 | This study | N/A |
| *pih1Δ* tet07-CNS1 Y8205 MATa can1::STE2pr-Sp-his5 lyp1::STE3pr-Sp-LEU2 his3-1 leu2-0 URA3::CMV-tTA pCNS1::natMX-tet07-TATA pih1::kanMX4 | This study | N/A |
| *cpr6Δ* tet07-CNS1 Y8205 MATa can1::STE2pr-Sp-his5 lyp1::STE3pr-Sp-LEU2 his3-1 leu2-0 URA3::CMV-tTA pCNS1::natMX-tet07-TATA cpr6::kanMX4 | This study | N/A |
| *cpr7Δ* tet07-CNS1 Y8205 MATa can1::STE2pr-Sp-his5 lyp1::STE3pr-Sp-LEU2 his3-1 leu2-0 URA3::CMV-tTA pCNS1::natMX-tet07-TATA cpr7::kanMX4 | This study | N/A |
| *aha1Δ* tet07-CNS1 Y8205 MATa can1::STE2pr-Sp-his5 lyp1::STE3pr-Sp-LEU2 his3-1 leu2-0 URA3::CMV-tTA pCNS1::natMX-tet07-TATA aha1::kanMX4 | This study | N/A |
| *hch1Δ* tet07-CNS1 Y8205 MATa can1::STE2pr-Sp-his5 lyp1::STE3pr-Sp-LEU2 his3-1 leu2-0 URA3::CMV-tTA pCNS1::natMX-tet07-TATA hch1::kanMX4 | This study | N/A |
| *ppt1Δ* tet07-CNS1 Y8205 MATa can1::STE2pr-Sp-his5 lyp1::STE3pr-Sp-LEU2 his3-1 leu2-0 URA3::CMV-tTA pCNS1::natMX-tet07-TATA ppt1::kanMX4 | This study | N/A |
| *sba1Δ* tet07-CNS1 Y8205 MATa can1::STE2pr-Sp-his5 lyp1::STE3pr-Sp-LEU2 his3-1 leu2-0 URA3::CMV-tTA pCNS1::natMX-tet07-TATA sba1::kanMX4 | This study | N/A |
| *cdc37-DAmP* tet07-CNS1 Y8205 MATa can1::STE2pr-Sp-his5 lyp1::STE3pr-Sp-LEU2 his3-1 leu2-0 URA3::CMV-tTA pCNS1::natMX-tet07-TATA cdc37-DAmP::kanMX4 | This study | N/A |
| WT Yeast BY4741; MATa; ura3Δ0; leu2Δ0; his3Δ1; met15Δ0; | Euroscarf | Cat# Y00000 |
| *sti1*Δ BY4741; MATa; ura3Δ0; leu2Δ0; his3Δ1; met15Δ0; YOR027w::kanMX4 | Euroscarf | Cat# Y01803 |
| *ppt1*Δ BY4741; MATa; ura3Δ0; leu2Δ0; his3Δ1; met15Δ0; YGR123cw::kanMX4 | Euroscarf | Cat# Y04753 |
| *sba1*Δ BY4741; MATa; ura3Δ0; leu2Δ0; his3Δ1; met15Δ0; YKL117w::kanMX4 | Euroscarf | Cat# Y04967 |
| *cpr6*Δ BY4741; MATa; ura3Δ0; leu2Δ0; his3Δ1; met15Δ0; YLR216c::kanMX4 | Euroscarf | Cat# Y04165 |
| *cpr7*Δ BY4741; MATa; ura3Δ0; leu2Δ0; his3Δ1; met15Δ0; YJR032w::kanMX4 | Euroscarf | Cat# Y06830 |
| *aha1*Δ BY4741; MATa; ura3Δ0; leu2Δ0; his3Δ1; met15Δ0; YDR214w::kanMX4 | Euroscarf | Cat# Y03573 |
| *hch1*Δ BY4741; MATa; ura3Δ0; leu2Δ0; his3Δ1; met15Δ0; YNL281w::kanMX4 | Euroscarf | Cat# Y01163 |
| *tah1*Δ BY4741; MATa; ura3Δ0; leu2Δ0; his3Δ1; met15Δ0; CR060w::kanMX4 | Euroscarf | Cat# Y07189 |
| *pih1*Δ BY4741; MATa; ura3Δ0; leu2Δ0; his3Δ1; met15Δ0; YHR034c::kanMX4 | Euroscarf | Cat# Y00997 |
| *cdc37*-DAmP BY4741; MATa; ura3Δ0; leu2Δ0; his3Δ1; met15Δ0; cdc37-DAmP::kanMX4 | Dharmacon | Cat# YSC5093-213595844 |
| *cns1*-DAmP BY4741; MATa; ura3Δ0; leu2Δ0; his3Δ1; met15Δ0; cns1-DAmP::kanMX4 | Dharmacon | Cat# YSC5093-21359678 |
| R1158 URA3::CMV-tTA MATa his3-1 leu2-0 met15-0 | Open Biosystems | N/A |
| *cpr7*Δ R1158 cpr7::natNT2 | This study | N/A |
| tet07-*CNS1* R1158 pCNS1::kanR-tet07-TATA | Dharmacon | Cat# TH3647 |
| tet07-*CNS1 cpr7*Δ R1158 pCNS1::kanR-tet07-TATA cpr7::natNT2 | This study | N/A |

(*Continued on next page*)

*Continued*

| REAGENT or RESOURCE | SOURCE | IDENTIFIER |
|---|---|---|
| R1158 MET+ URA3::CMV-tTA MATa his3-1 leu2-0 MET15 | This study | N/A |
| *cpr7*Δ MET+ R1158 cpr7::natNT2 MET15 | This study | N/A |
| tet07-*CNS1* MET+ R1158 pCNS1::kanR-tet07-TATA MET15 | This study | N/A |
| tet07-*CNS1 cpr7* Δ MET+ R1158 pCNS1::kanR-tet07-TATA cpr7::natNT2 MET15 | This study | N/A |
| Y8205 MATalpha can1::STE2pr-Sp-his5 lyp1::STE3pr-Sp-LEU2 his3-1 leu2-0 ura3-0 | This study | N/A |
| Y8205 *cpr7*Δ MATalpha can1::STE2pr-Sp-his5 lyp1::STE3pr-Sp-LEU2 his3-1 leu2-0 ura3-0 cpr7::natMX | This study | N/A |
| Y8205 tet07-*CNS1* MATalpha can1::STE2pr-Sp-his5 lyp1::STE3pr-Sp-LEU2 his3-1 leu2-0 URA3::CMV-tTA pCNS1::natMX-tet07-TATA | This study | N/A |
| Y8205 tet07-*CNS1 cpr7*Δ MATalpha can1::STE2pr-Sp-his5 lyp1::STE3pr-Sp-LEU2 his3-1 leu2-0 URA3::CMV-tTA pCNS1::natMX-tet07-TATA cpr7::hygNT1 | This study | N/A |
| R1158 *sgt1*-DAmP URA3::CMV-tTA MATa his3-1 leu2-0 met15-0 sgt1-DAmP::hygNT1 | This study | N/A |
| cpr7Δ *sgt1*-DAmP R1158 cpr7::natNT2 sgt1-DAmP::hygNT1 | This study | N/A |
| tet07-*CNS1 sgt1*-DAmP R1158 pCNS1::kanR-tet07-TATA sgt1-DAmP::hygNT1 | This study | N/A |
| tet07-*CNS1 cpr7*Δ *sgt1*-DAmP R1158 pCNS1::kanR-tet07-TATA cpr7::natNT2 sgt1-DAmP::hygNT1 | This study | N/A |
| Recombinant DNA | | |
| p425-GPD Cns1-WT | This study | N/A |
| p425-GPD Sti1-WT | A. Röhl | N/A |
| p415-GALS HA-eEF2 | This study | N/A |
| pET28-SUMO Cns1-1-190 | This study | N/A |
| pET28-SUMO Cns1-51-385 | This study | N/A |
| pET28-SUMO Cpr7 | This study | N/A |
| p426-GPD Cns1-WT (URA3) | This study | N/A |
| p425-GPD Cns1 1-200 | This study | N/A |
| p425-GPD Cns1 1-190 | This study | N/A |
| p425-GPD Cns1 1-185 | This study | N/A |
| p425-GPD Cns1 219-385 | This study | N/A |
| p425-GPD Cns1 36-385 | This study | N/A |
| p425-GPD Cns1 41-385 | This study | N/A |
| p425-GPD Cns1 46-385 | This study | N/A |
| p425-GPD Cns1 51-385 | This study | N/A |
| p425-GPD Cns1 36-205 | This study | N/A |
| p425-GPD Cns1 36-200 | This study | N/A |
| p425-GPD Cns1 36-195 | This study | N/A |
| p425-GPD Cns1 1-82 | This study | N/A |
| p425-GPD Cns1 1-220 | This study | N/A |
| p425-GPD Cns1 191-385 | This study | N/A |
| p425-GPD 1-82-L-169-385 | This study | N/A |
| p425-GPD 1-82-L | This study | N/A |
| p425-GPD 1-82-L-191-385 | This study | N/A |
| p425-GPD 1-82-L-191-220 | This study | N/A |
| p425-GPD Cns1 221-385 | This study | N/A |
| p425-GPD 1-82-L-221-385 | This study | N/A |
| p425-GPD TTC4 | This study | N/A |

(*Continued on next page*)

*Continued*

| REAGENT or RESOURCE | SOURCE | IDENTIFIER |
|---|---|---|
| p425-GPD Cns1N/TTC4 | This study | N/A |
| p425-GPD Hsc82 | This study | N/A |
| p425-GPD Hsc82-Cns1-1-82 | This study | N/A |
| p425-GPD Cns1-1-82-Hsc82 | This study | N/A |
| p425-GPD Ssa1 | This study | N/A |
| p425-GPD Ssa1-Cns1-1-82 | This study | N/A |
| p425-GPD Cns1 1-82-TPR1 | This study | N/A |
| p425-GPD Cns1 1-82-TPR2A | This study | N/A |
| p425-GPD Cns1 1-82-TPR2B | This study | N/A |
| p425-GPD Sti1 TPR1 | A. Röhl | N/A |
| p425-GPD Sti1 TPR2A | A. Röhl | N/A |
| p425-GPD Sti1 TPR2B | A. Röhl | N/A |
| pET28-SUMO Cns1-WT | This study | N/A |
| pET28-SUMO Cns1-36-385 | This study | N/A |
| pET28-SUMO Cns1-1-82 | This study | N/A |
| pET28-SUMO Cns1-169-385 | This study | N/A |
| pET28-SUMO Cns1-36-205 | This study | N/A |
| pET28-SUMO Cns1-70-205 | This study | N/A |
| pET28-SUMO Cns1-70-220 | This study | N/A |
| pET28-SUMO Cns1-221-385 | This study | N/A |
| pET28-SUMO Cns1-1-220 | This study | N/A |
| pET28-SUMO Cns1-36-220 | This study | N/A |
| pET28-SUMO Cns1-1-82-L-221-385 | This study | N/A |
| pET28-SUMO TTC4 | This study | N/A |
| pET28-SUMO Cns1N/TTC4 | This study | N/A |
| pET28-SUMO TTC4-217-387 | This study | N/A |
| pET28-SUMO Cns1-70-385 | This study | N/A |
| pET28-SUMO Cns1-70-190 | This study | N/A |
| pET28-SUMO Hgh1 | This study | N/A |
| p413-GAL1 TEF1 | This study | N/A |
| p413-GAL1 eEF2 | This study | N/A |
| p413-GAL1 YEF3 | This study | N/A |
| p413-GAL1 HYP2 | This study | N/A |
| p413-GAL1 SUP35 | This study | N/A |
| p413-GAL1 SUP45 | This study | N/A |
| Software and Algorithms | | |
| OriginPro9 | Originlab | N/A |
| ImageJ | ImageJ developers | N/A |

## CONTACT FOR REAGENT AND RESOURCE SHARING

Further information and requests for resource and reagents should be directed to and will be fulfilled by the Lead Contact, Prof. Dr. Johannes Buchner (johannes.buchner@tum.de).

## EXPERIMENTAL MODEL AND SUBJECT DETAILS

### Yeast strains

Yeast strains used in this study are derivatives of BY4741 (MATa his3Δ1 leu2Δ0 met15Δ0 ura3Δ0) and were obtained from Euroscarf. The yeast strains, generated in this study, were obtained by linear transformation or generated using the SGA method. Yeast cells

were plated on YPD plates and cultured in liquid media. Strains transformed with auxotrophic vectors were grown on the respective auxotrophic minimal medium. Cells were grown at 30°C, unless specified otherwise.

## METHOD DETAILS

### Protein purification

Cns1 and TTC4 and mutants thereof as well as Hgh1 and Cpr7 were expressed in *E. coli* as N-terminal 6xHis-SUMO fusion proteins. Cells were lysed in 40 mM $K_2HPO_4/KH_2PO_4$ pH 7.5, 300 mM KCl, 20 mM imidazole, 1 mM DTT + protease inhibitor G (Serva) + 2 mM PMSF. Lysates were cleared at 40,000 g for 1 h. Cleared lysates were run over a His-Trap FF column (GE Healthcare) followed by a washing step with 10 column volumes 97% 40 mM $K_2HPO_4/KH_2PO_4$ pH 7.5, 300 mM KCl, 20 mM imidazole, 1 mM DTT and 3% $K_2HPO_4/KH_2PO_4$ pH 7.5, 300 mM KCl, 500 mM imidazole, 1 mM DTT. The fusion protein was the eluted in a one-step elution with 100% 40 mM $K_2HPO_4/KH_2PO_4$ pH 7.5, 300 mM KCl, 500 mM imidazole, 1 mM DTT. Next, the buffer was exchanged to 40 mM HEPES pH 7.5, 150 mM KCl, 5 mM $MgCl_2$, 1 mM DTT using a HiPrep 26/10 desalting column (GE Healthcare), His-tagged SUMO protease was added and the protein was cleaved at 4°C over night. To get rid of the SUMO tag and the protease, the digested protein prep was run again over a His-Trap FF column and the flow through was collected. Finally, the proteins were applied to a Superdex 200 Prep Grade column (GE Healthcare) equilibrated in 40 mM HEPES pH 7.5, 150 mM KCl, 5 mM $MgCl_2$, 1 mM DTT and purity was checked by SDS-PAGE and Coomassie staining. For the isotopically labeled proteins used in NMR experiments, cells were grown in M9 media supplemented with $^{15}NH_4Cl$ and $^{13}C_6$ D-glucose when needed. Proteins were expressed and purified as described except in the last gel filtration chromatography, in which 20 mM $Na_2HPO_4/NaH_2PO_4$ pH 7.4, 100 mM NaCl, 5 mM mM DTT and 0.02% $NaN_3$ (NMR buffer) was used. For the $Cns1^{1-190}$ and $Cns1^{70-205}$ constructs, an additional resource Q anion exchange chromatography was performed after the gel filtration.

For TTC4 and the Cns1N/TTC4 chimera, an additional ion exchange step was necessary. After the first His-Trap column the eluate was diluted 1:20 in Resource Q buffer A (40 mM $K_2HPO_4/KH_2PO_4$ pH 7.5, 10 mM KCl, 1 mM DTT) and samples were loaded onto a Resource Q column (GE Healthcare). After washing with 10 column volumes Resource Q buffer A, proteins were eluted with a continuous gradient from Resource Q buffer A to 50% Resource Q buffer B (40 mM $K_2HPO_4/KH_2PO_4$ pH 7.5, 1 M KCl, 1 mM DTT) over 200 ml. Buffer exchange, SUMO protease digestion, reverse Ni chromatography and gel filtration were carried out as described above for Cns1 and Hgh1.

Hsp90 was purified as described previously using NiNTA chromatography followed by resource Q anion exchange chromatography, hydroxyapatite ion exchange chromatography and size exclusion chromatography (Richter et al., 2001).

eEF2 was purified using a modified protocol described previously (Ortiz et al., 2006). TKY675 yeast cells (Kerafast) expressing C-terminally His-tagged eEF2 were grown in YPD to $OD_{600}$ = 1.5, harvested by centrifugation and lysed in 40 mM $K_2HPO_4/KH_2PO_4$ pH 7.5, 1 M KCl, 20 mM imidazole, 1 mM DTT, protease inhibitor HP (Serva) 2 mM PMSF, 1% Tween 20. The lysate was cleared by centrifugation at 50,000 rpm for 1 h filtered through a 0.45 μm filter and applied to a His-Trap FF column (GE Healthcare). After extensive washing with lysis buffer the protein was eluted in 40 mM $K_2HPO_4/KH_2PO_4$ pH 7.5, 1 M KCl, 300 mM imidazole 1 mM DTT. The pooled fractions were then run over a Superdex 200 26/60 column equilibrated in 20 mM Tris-HCl pH 8, 100 mM KCl, 0.1 mM EDTA, 10% glycerol, 1 mM DTT and finally the protein was dialyzed into 40 mM HEPES pH 7.5, 150 mM KCl, 5 mM $MgCl_2$, 1 mM DTT.

### Protein fluorescent labeling

Proteins used in analytical ultracentrifugation were labeled as follows: Cns1 was labeled with Atto488-NHS using a 1:1 protein/dye ratio. Hgh1 was labeled with Atto488-maleimide using a 1:2 protein/dye ratio and eEF2 was labeled using Atto488-maleimide using a 1:1.4 protein/ dye ratio. Labeling was performed in 40 mM HEPES pH 7.5, 150 mM KCl, 5 mM $MgCl_2$ for 1 h at room temperature.

### Tandem affinity purification

Cns1 interactors were co-purified using a modified protocol of the TAP method (Puig et al., 2001). A yeast strain carrying C-terminally TAP-tagged Cns1 was grown in 2 L YPD medium to a $OD_{600}$ ~3. Cells were harvested by centrifugation; pellets were frozen in liquid nitrogen and stored at −80°C before further processing. Cells were lysed in 50 mM Tris-HCl, 50 mM NaCl, 1.5 mM $MgCl_2$, 0.15% NP-40, 1 mM DTT by glass bead disruption, lysates were cleared by centrifugation and the resulting supernatant was incubated with 100 μL IgG beads for one h. After washing with lysis buffer and TEV cleavage the eluate was recovered by gravity flow and separated by SDS-PAGE. Cns1 interactors were identified by mass spectrometry.

### Protein identification by mass spectrometry

The gel was cut into 6 pieces and an in-gel digestion (Shevchenko et al., 2006) was performed using trypsin as digestion enzyme. Mass spectrometry was performed on an LTQ Orbitrap Velos mass spectrometer (Thermo Fisher Scientific, Germany) connected to a nanoLC Ultra 1D liquid chromatography system (Eksigent, CA) using an in-house packed precolumn (20 mm x 75 μm ReproSil-Pur C18, Dr. Maisch, Germany) and analytical column (400 mm x 50 μm ReproSil-Pur C18, Dr. Maisch, Germany) using 60 min of analysis time for each sample. Full-scan mass spectrometric spectra were acquired in the Orbitrap at 30,000 resolution. The five most intense precursors were selected for HCD fragmentation (isolation width, 2.0 Th) with a normalized collision energy

of 40% at an AGC target setting of 50,000. HCD spectra were acquired in the Orbitrap at 7,500 resolution. Peak lists were generated from raw MS data files using Mascot Distiller v2.4.3.1 (Matrix Science, UK) and were searched using Mascot (Matrix Science, London, UK; version 2.4.1). Mascot was set up to search the 000000_SwissProt_v57_15_033010 database (selected for *Saccharomyces cerevisiae*, 6973 entries) assuming the digestion enzyme trypsin. Fragment ion mass tolerance was set to 0.05 Da and a parent ion tolerance was 10.0 ppm. Carbamidomethyl of cysteine was specified as a fixed modification. Oxidation of methionine, acetyl of lysine and the N terminus and phospho of serine, threonine and tyrosine were specified in Mascot as variable modifications. The search results were loaded into Scaffold (version Scaffold_4.8.6, Proteome Software, Portland, OR) to validate MS/MS based peptide and protein identifications. Peptide identifications were accepted if they could be established at greater than 97.0% probability by the Scaffold Local FDR algorithm. Protein identifications were accepted if they could be established at greater than 92.0% probability to achieve an FDR less than 1.0% and contained at least 1 identified peptide. Protein probabilities were assigned by the Protein Prophet algorithm (Nesvizhskii et al., 2003). Proteins that contained similar peptides and could not be differentiated based on MS/MS analysis alone were grouped to satisfy the principles of parsimony. Proteins sharing significant peptide evidence were grouped into clusters.

## Crystallization and structure determination

Cns1$^{221\text{-}385}$ was crystallized at 20°C from a 1:1 mixture of protein (15-20 mg/mL) and reservoir by the sitting drop vapor diffusion technique. Native crystals grew from solutions containing 0.1 M 2-(*N*-morpholino)ethanesulfonic acid (MES) pH 6.5 and 25% (v/v) polyethylene glycol (PEG) 3000, while selenomethionine labeled protein crystallized from 0.1 M 4-(2-hydroxyethyl)-1-piperazineethanesulfonic acid (HEPES) pH 7.5, 10% (v/v) isopropanol and 20% (v/v) PEG4000. Crystals were cryoprotected by 25% (v/v) PEG400. Native and anomalous datasets were recorded at $\lambda = 1.0$ Å and the peak wavelength of Se ($\lambda = 0.9794$ Å), respectively. Data processing and reduction was performed with the program package XDS (Kabsch, 2010). Within the CRANK2 (Pannu et al., 2011) pipeline (CCP4) for automated SAD phasing, SHELXD identified 10 Se sites, which subsequently allowed for automated model building and almost complete models for the two Cns1$^{221\text{-}385}$ molecules per asymmetric unit. Upon refinement against the native high-resolution dataset, final model building was carried out with Coot (Emsley et al., 2010).

Crystals of the C domain of human TTC4 (amino acid residues 217-387) were grown at 20°C in sitting drop plates. Droplets contained equal volumes of protein (15 mg/mL) and reservoir solutions (1.4 M Na/K phosphate pH 8.2). Crystals were cryoprotected by the addition of a 1:1 (v/v) mixture of mother liquor and 60% (v/v) glycerol. Phases were obtained by molecular replacement calculations with Phaser (McCoy et al., 2007) using the coordinates of Cns1$^{221\text{-}385}$ (PDB ID 6HFM) as a search model. After restrained refinements with REFMAC5 (Vagin et al., 2004), the initial model was rebuilt with Coot (Emsley et al., 2010).

Crystals of Cns1$^{70\text{-}385}$ grew at 20°C from sitting drop vapor diffusion trials. Droplets contained a 1:1 ratio of protein (20 mg/mL) and 0.1 M tris(hydroxymethyl)aminomethane (Tris) /HCl pH 8.5, 25% (v/v) PEG3000. Crystals were cryoprotected by 25% (v/v) PEG200. Diffraction data were collected at $\lambda = 0.97793$ Å and processed by XDS (Kabsch, 2010). Patterson search calculations with Phaser (McCoy et al., 2007) using Cns1$^{221\text{-}385}$ as a search model (PDB ID 6HFM) positioned one molecule per asymmetric unit. After restrained refinements with REFMAC5 (Vagin et al., 2004) additional $2F_O\text{-}F_C$ electron density was observed at the N terminus of the Cns1$^{221\text{-}385}$ model. Iterative model building (Coot (Emsley et al., 2010)) and refinement steps (REFMAC5 (Vagin et al., 2004)) allowed tracing of the entire Cns1$^{70\text{-}385}$ construct except for the N-terminal four amino acids.

Upon completion of all models, water molecules were automatically placed with ARP/wARP solvent (Perrakis et al., 1997). Translation/libration/screw (TLS) refinements with REFMAC5 (Vagin et al., 2004) finally yielded excellent R factors and geometry values for all three crystal structures (Table 1). The coordinates were proven to fulfil the Ramachandran plot using PROCHECK (Laskowski et al., 1993) and validated by MolProbity (Chen et al., 2010). Structure factors and model coordinates were deposited in the RCSB Protein Data Bank. The respective accession codes are provided in Table 1.

## NMR spectroscopy

NMR spectra were recorded at 298 K using Bruker AV600, 900 and 950 MHz spectrometers equipped with cryogenically cooled probes. In all constructs, protein concentrations were around 300 μM in NMR buffer. 2D $^{1}H$, $^{15}N$ watergate-flip-back HSQC experiments were used for the Cns1$^{1\text{-}82}$, Cns1$^{1\text{-}190}$ and Cns1$^{70\text{-}205}$ constructs. Sequence-specific assignment of $^{1}HN$, $^{15}N$, $^{13}C\alpha$, $^{13}C\beta$ and $^{13}C'$ backbone resonances was achieved by HNCACB, CBCAcoNH, HNCA, HNcoCA, HNCO and HNcaCO experiments (Sattler et al., 1999). In all cases, non-uniform sampling was employed. {$^{1}H$}-$^{15}N$ heteronuclear NOE values were obtained by recording spectra with and without $^{1}H$ saturation before the starting of the experiment, and comparing the intensities (Farrow et al., 1994a). Spectra were processed by Bruker Topspin 3.5 software (Bruker, Billerica, USA) and further analyzed using CcpNmr (Vranken et al., 2005). $^{1}H$-$^{15}N$ combined chemical shifts were calculated with the following formula:

$$\Delta\delta_{N,H}(ppm) = \sqrt{\Delta\delta_H^2 + (\alpha \bullet \Delta\delta_N)^2}$$

Where $\alpha$ is the ratio of the differences between the maximal and minimal $^{1}H$ and $^{15}N$ chemical shifts of protein signals (in ppm). In interaction experiments, 1.1 – 1.2 molar excess of the unlabeled partner was used in all cases, except for MEEVD peptide, in which a saturating concentration of 5 mM was used.

### Small Angle X-ray Scattering

SAXS data for solutions of full-length Cns1, Cns1$^{1-220}$, Cns1$^{70-220}$, Cns1$^{36-220}$ were recorded on a SAXS instrument (SAXSess mc2, Anton Paar, Graz, Austria) equipped with a Kratky camera, a sealed X-ray tube source and a two-dimensional Princeton Instruments PI•SCX:4300 (Roper Scientific) CCD detector. The scattering patterns were measured with 90-min exposure times (540 frames, each 10 s) at a concentration of 5.0 mg/mL. Radiation damage was excluded based on a comparison of individual frames of the 90-min exposures, where no changes were detected. A range of momentum transfer of $0.012 < s < 0.63$ Å-1 was covered ($s = 4\pi \sin(\theta)/\lambda$, where $2\theta$ is the scattering angle and $\lambda = 1.542$ Å is the X-ray wavelength).

All SAXS data were analyzed with the package ATSAS (version 2.5). The data were processed with the SAXSQuant software (version 3.9), and desmeared using the programs GNOM and GIFT. The forward scattering, I(0), the radius of gyration, $R_g$, the maximum dimension, $D_{max}$, and the inter-atomic distance distribution functions, (P(R)), were computed with the program GNOM. The masses of the solutes were evaluated by comparison of the forward scattering intensity with that of a human serum albumin reference solution (molecular mass 69 kDa) and using Porod's law.

The theoretical SAXS curve was calculated from the crystal structure using the program CRYSOL (Svergun et al., 1995).

P(r) functions obtained from GNOM (Semenyuk and Svergun, 1991) were subsequently used by DAMMIF (Franke and Svergun, 2009) to generate 50 *ab initio* models for each construct. DAMAVER (Volkov and Svergun, 2003) was then used to generate an average model and DAMCLUST (Petoukhov et al., 2012) to cluster similar models into groups. Generated models were then fitted with previous obtained crystal structure of Cns1 using PyMOL (Version 2.2.0, Schrodinger LLC).

The structures of Cns170-385 with different linker lengths were modeled using the program CORAL (Petoukhov and Svergun, 2005). Input was the high-resolution crystal structures of Cns1 determined here and experimental SAXS data. Structures were calculated using flexible linkers within the region of residue 201 to 224 in Cns1.

### Hydrogen/deuterium exchange (H/DX)

Hydrogen/deuterium exchange experiments (H/DX) were performed using an ACQUITY UPLC M-class system equipped with automated H/DX technology (Waters) as described previously (Boczek et al., 2015; Rosam et al., 2018). In short, H/DX kinetics were determined by taking data points at 0, 10, 60, 600, 1800 and 7200 s at 20 °C. At each data point of the kinetic, 3 μl of a solution of 15 μM of eEF2, Cns1 or Hgh1 was extracted and analyzed. When the dynamics of eEF2, Cns1 or Hgh1 in the complex with Cns1 or Hgh1 were studied, 3 μl of a mixture of 15 μM eEF2, Cns1 or Hgh1 and 75 μM Cns1 or Hgh1 were analyzed at each time point of the kinetics. After H/D exchange, the samples were digested on a Waters Enzymate BEH pepsin column 2.1 × 30 mm. Peptides were separated by reverse phase chromatography using a Waters Acquity UPLC C18 1.7 μm Vangard 2.1 × 5 mm precolumn and a Waters Aquity UPLC BEH C18 1.7 μm 1 × 100 mm separation column and the eluted peptides were analyzed using an in-line Synapt G2-S QTOF HDMS mass spectrometer (Waters). Deuterium levels were not corrected for back exchange and are therefore reported as relative deuterium levels. MS data were collected over an m/z range of 100–2,000. Mass accuracy was ensured by calibration and peptides were identified by triplicate $MS^E$. Data were analyzed with the PLGS 3.0.3 and DynamX 3.0 software packages.

### Analytical ultracentrifugation

Analytical ultracentrifugation experiments were performed using a ProteomLab Beckman XL-A centrifuge (Beckman Coulter, Brea, California) equipped with an AVIV fluorescence detection system (Aviv biomedical, Lakewood, USA) using 500 nM labeled protein. 40 mM HEPES pH 7.5, 50 mM KCl, 5 mM $MgCl_2$ was used as measurement buffer. Nucleotides (ATP, ADP, AMP-PNP) were added at 2 mM. Samples were filled in quartz-capped charcoal-filled epon double sector centerpieces with an optical path length of 12 mm. Experiments were performed at 42,000 rpm and 20°C in an eight-hole Ti-50 Beckman-Coulter rotor. Sedfit (Schuck, 2000) and OriginPro 9 were used for data analysis.

### Yeast mutant strain construction, 5′-FOA shuffling and spot assays

All yeast strains were transformed using the lithium acetate/PEG transformation method (Gietz and Woods, 2002). The *CNS1* shuffling strain *cns1Δ* [CNS1] was constructed by transforming the heterozygous diploid CNS1/cns1Δ strain with the p426-GPD-CNS1 plasmid carrying a *URA3* marker. After sporulation, tetrads were picked and haploid cells carrying a genomic CNS1 knockout and the CNS1 expressing URA3 plasmid were selected. The resulting strain was used in 5′-FOA shuffling experiments by transforming it with p425-GPD plasmids (SD -LEU selection) carrying truncation and mutant variants of CNS1 to investigate cell growth after loss of the URA3/CNS1 wt plasmid.

The yeast strains *cpr7Δ* and tet07-*CNS*1 *cpr7*Δ were constructed by linear knockout of the *Cpr7* wt gene following a method described before (Janke et al., 2004). *hgh1* strains were constructed by linear knockout of HGH1 as mentioned for *cpr7*. The methionine prototroph strains (MET+) used in radioactive translation assays were constructed by amplifying the MET25 wild-type gene from BY4742 by PCR. The PCR product was then transformed into the respective strains and mutants were selected for growth on SD -MET medium.

Double mutants of tet07-CNS1 and *cpr7Δ* with Hsp90 co-chaperone mutant strains and the *hgh1Δ* strain were constructed by random spore analysis as described previously (Tong and Boone, 2007) by using yeast strains Y8205 *cpr7Δ*, Y8205 tet07-CNS1

and Y8205 tet07-CNS1 *cpr7Δ*. Only the sgt1-DAmP strain was constructed by genomic integration of the hygromycin B resistance cassette in the 3′-UTR of SGT1 as described previously (Breslow et al., 2008). For spot assays, 5 μL were spotted as 10-fold dilutions starting from $OD_{600}$ = 1.

### Ribosome fractionation, polysome run-off analysis, sample precipitation for western blot

Yeast cells were grown in YPD medium in the presence or absence of doxycyline at 30°C to a $OD_{600}$ = 0.8. Before harvesting the cells were treated either for 10 min with cycloheximide or starved for 10 min in medium lacking glucose (yeast extract, peptone). 160 $OD_{600}$ units were harvested by centrifugation and cell pellets were frozen in liquid nitrogen and stored at −80°C before further processing. Lysates were prepared in 10 mM Tris-HCl pH 7.5, 100 mM NaCl, 30 mM $MgCl_2$, 1 mM DTT, 100 μg/mL cycloheximide and protease inhibitor cocktail (Roche) in a FastPrep-24 homogenizer (MP Biomedicals). Subsequent ribosome fractionation on a continuous 7%–47% sucrose gradient was carried out as described previously (Choe et al., 2016). Finally, $A_{254}$ nm recordings and sample fractionation were carried out using a piston gradient fractionator coupled to a spectrophotometer (Biocomp).

For western blots, 10 μL 2% (w/v) sodiumdeoxycholat was added to each fraction, proteins were precipitated by adding 100 μL 100% (w/v) TCA followed by 60 min incubation on ice. Pellets were washed twice with 80% (v/v) acetone and resuspended in SDS sample buffer.

The polysome/monosome ratio was determined by calculating the area underneath the 80S peak and the polysome peaks using Origin Pro 9 and dividing the polysome area by the 80S monosome area.

### $^{35}$S methionine labeling to quantify total protein translation in vivo

To quantify *in vivo* protein synthesis we used a modified protocol described previously (Esposito and Kinzy, 2014). In brief, methionine prototroph yeast mutants were grown at 30°C in SD -MET medium containing 10 μg/mL doxycycline to $OD_{600}$ = 0.8. 10 $OD_{600}$ units were harvested by centrifugation and resuspended in 10 mL pre-warmed SD -MET+dox medium. 7 μL "hot" methionine mix (5 μl 10 mM cold methionine + 2 μL "hot" methionine per 1 mL culture) were added and cells were further grown at 30°C. After 30 and 60 min, respectively, cycloheximide (100 μg/mL) was added to stop the reaction. Cells equivalent to 1 $OD_{600}$ were harvested. Proteins were extracted by using an alkali lysis protocol (Kushnirov, 2000). Proteins were separated by SDS-PAGE and autoradiography was analyzed using a Typhoon 4000 multimode scanner.

### Analysis of eEF2 aggregation *in vivo*

To separate aggregated from soluble eEF2, cells were grown to logarithmic phase in the presence of 10 μg/mL Doxycyclin. Subsequently, 40 OD units were harvested, washed with PBS and then resuspended in 500 μl Lysis Buffer (50 mM Tris, pH 8.0, 150 mM NaCl, 5 mM $MgCl_2$, 5% glycerol) supplemented with 1x Protease Inhibitor Mix G (Serva), 1 mM PMSF, 12.5 units of Benzonase (Sigma-Aldrich), 5 mM EDTA and 2 μg/mL puromycin. Cells were disrupted by glass-bead disruption, suspension was cleared by mild centrifugation at 500 x g for 1 min at 4°C. Protein concentration was then normalized by Bradford assay in triplicates and 50 μl of the normalized sample volume were pelleted at 18,000 x g at 4°C, the supernatant was aspirated and the pellet was washed twice with lysis buffer. Subsequently, the pellet was resuspended in resuspension buffer (1% SDS, 6 M urea, 50 mM Tris-HCl, pH 7.5, 1 mM EDTA) and samples were subjected to SDS-PAGE and Western-Blotting following standard procedures.

### Hsp90 inhibition in vivo

Cells harboring the p415GAL-S HA-eEF2 plasmid were grown to logarithmic phase in selective media with 2% raffinose as carbon source. Cells were treated with 25 μM Radicicol or DMSO before eEF2 expression was induced by addition of a final concentration of 2% (w/v) D-galactose. Samples were taken at the indicated time points and lysed by an alkali lysis protocol (Kushnirov, 2000). Samples were then separated by SDS-PAGE and analyzed by Western-Blot following standard techniques.

## QUANTIFICATION AND STATISTICAL ANALYSIS

Statistical parameters are reported in the figures and figure legends. Statistical significance was assigned by using a two-sample t test. P values below 0.05 were classified as significant (*). Statistical analyses were performed using OriginPro 9. For specific methods the respective software used is mentioned in the STAR methods.

## DATA AND SOFTWARE AVAILABILITY

The crystal structure Cns1$^{221\text{-}385}$, TTC4$^{217\text{-}385}$ and the crystal structure of Cns1$^{70\text{-}385}$ have been deposited in the Protein Data Bank (PDB) under ID codes 6HFM, 6HFO and 6HFT. All datasets used for this study are available from the corresponding author upon reasonable request.